AC SAF IASI/MetopA & IASI/MetopB

Sulphur Dioxide Validation Report
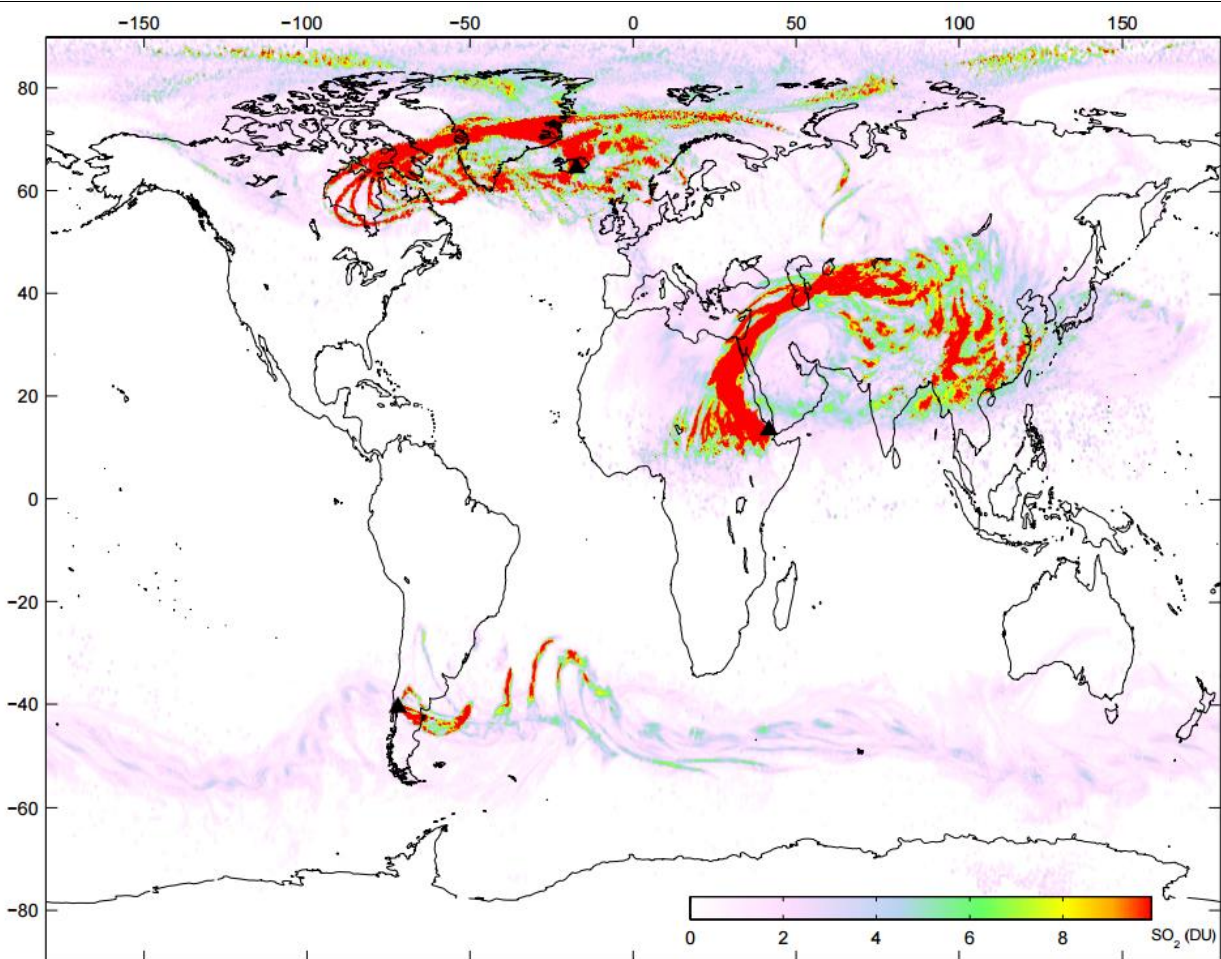
Composite image of maximum observed SO₂ for the Grimsvotn [May 21st], Puyehue-Cordon Caulle [3rd June] and Nabro [12th June] eruptions in 2011. Image courtesy of Clarisse et al., 2012, Fig.12.

VALIDATED PRODUCTS:

Identifier	Name	Acronym
O3M-57	IASI/MetopA &/MetopB Sulphur Dioxide Column	IASI-A SO2

AUTHORS:

Main authors:	Institute
MariLiza Koukouli	Aristotle University of Thessaloniki | LAP/AUTH
Gaia Pinardi	Royal Belgian Institute for Aeronomy | BIRA
Contributing authors:	
Maya George	Laboratoire Atmosphères, Milieux, Observations Spatiales | LATMOS
Nicolas Theys	Royal Belgian Institute for Aeronomy | BIRA
Lieven Clarisse	Université Libre de Bruxelles | ULB
Rosa Astoreca	Université Libre de Bruxelles | ULB
Internal reviewers:	
Dimitris Balis	Aristotle University of Thessaloniki | LAP/AUTH
Michel van Roozendael	Royal Belgian Institute for Aeronomy | BIRA
Cathy Clerbaux	Laboratoire Atmosphères, Milieux, Observations Spatiales | LATMOS

Reporting period : IASI/MetopA SO$_2$: January 2007 – December 2013

IASI/MetopA SO$_2$: June 2017 – October 2017

IASI/MetopB SO$_2$: June 2017 – October 2017

Data processor versions:	**BRESCIA_v201510** **IASI OFL AERIS and IASI NRT_PPF_v6.3**

AC SAF VALIDATION REPORT FOR

IASI/METOPA AND IASI/METOPB

BRESCIA_201510

TOTAL SULPHUR DIOXIDE COLUMNS

This report is co-authored by *MariLiza Koukouli* and *Gaia Pinardi*
unless explicitly stated otherwise.

CONTENTS

ACRONYMS AND ABBREVIATIONS

ACSAF	Atmospheric Composition Satellite Application Facility
AERIS	Data Centre of the French Atmosphere Infrastructure
AUTH	Aristotle University of Thessaloniki
BRESCIA	Fast Optimal Retrievals on Layers for IASI
BTD	Brightness Temperature Difference
CDOP	Continues Development and Operations Proposal
D.U.	Dobson Unit
DOAS	Differential Optical Absorption Spectroscopy
ECMWF	European Centre for Medium-Range Weather Forecast
EUMETSAT	European Organisation for the Exploitation of Meteorological Satellites
HDF	Hierarchical Data Format
IASI	Infrared Atmospheric Sounding Interferometer
LATMOS	Laboratoire Atmosphères, Milieux, Observations Spatiales
MetOp	Meteorological Operational satellite
NRT	Near Real Time
OFL	Offline
OMI	Ozone Monitoring Instrument
SZA	Solar Zenith Angle
ULB	Université Libre de Bruxelles
WOUDC	World Ozone and UV Data Center
δBT	Brightness Temperature Difference

APPLICABLE AC SAF DOCUMENTS

[ATBD]   Brescia ATBD, issue 1, 23/06/2016, SAF/O3M/ULB/BresciaSO2_ATBD

[PUM]   Product User Manual for Near real-time IASI Brescia SO$_2$, Issue 1, 2/05/2017, SAF/AC/ULB/PUM/002

[PRD]   Product Requirements Document, SAF/AC/FMI/RQ/PRD/001, issue 1.1, 07/09/2017, D. Hovila, S. Hassinen, D. Loyola, P. Valks, J., S. Kiemle, O. Tuinder, H. Joench-Soerensen, F. Karcher, 2017.

EXECUTIVE SUMMARY

In the framework of EUMETSAT's Satellite Application Facility on Atmospheric Composition Monitoring (AC SAF, formerly O3M SAF), SO_2 total column data products have been generated using the Brescia v201510 algorithm operating at both LATMOS and EUMETSAT facilities as observed by the IASI instrument on board the MetOp-A and B platforms.

This report investigates the quality of the IASI/MetopA (2007-2013) and IASI/MetopA & /MetopB (June – October 2017) SO_2 columns by comparing them to ground-based measurements performed on a global scale by Brewer and MAXDOAS spectrophotometers, as well as satellite observations obtained by the OMI/Aura and GOME2/MetopA instruments. Different spatiotemporal collocation criteria were applied depending on the comparisons as well as different restriction criteria. The report is focused solely on SO_2 of volcanic provenance, and mainly from eruptive events at that.

The following main conclusions may be drawn:

- Out of fifty Brewer spectrophotometers that report SO_2 loading globally, 35 had collocations within 50km from an IASI overpass. Due to the locations of the most active volcanoes in remote areas, few Brewer instruments were able to capture SO_2 plumes created by the major volcanic events of the 2007-2013. It is shown that while the signal of the ground-based measurement rises above the noise levels inherent in the Brewer algorithm, those levels never reach the satellite reported ones [also seen in comparison with other satellite instruments.]

- Out of seven MAXDOAS spectrophotometers deployed globally, three provide meaningful collocations to the IASI overpasses, the ground-based stations generally show enhanced SO_2 signals just before/during/after the enhanced IASI SO_2 overpasses and the order of magnitude of the SO_2 signals is well comparable.

- Note that most of the validation results were made with the offline (ULB-LATMOS OFL AERIS) data product, which is in excellent agreement with the EUMETSAT NRT_PPF_v6.3 product, which was made operationally available to the validation teams since June 20th 2017 (see Section 1.2). The recommendation to filter the SO_2 NRT data according to Section 5.2.2 of the PUM has been followed in this Validation Report and remains up to date after the validation exercise (to only look at the retrievals in the neighbourhood of SO2_BT_DIFFERENCE>1K pixels, and not use the pixels with a SO2_BT_difference of less than 0.4K).

- Eleven major eruptive events were analysed in detail vis-a-vis the loadings observed by IASI/MetopA & /MetopB in comparison to OMI/Aura and GOME2/MetopA. Different assumptions in plume heights within the equivalent algorithms were all considered. The analysis on SO_2 masses showed that, for the entire eruption episodes, the correlations range between 0.70 and 0.95 depending on the plume height and satellite instrument. The IASI 13 & 16km plumes show the best agreement to the OMI/Aura 15km plume mostly around ±20%.

- The results are within the user requirements as stated in the Product Requirements Document [PRD]: Threshold accuracy: 200%; Target accuracy: 100%; Optimal accuracy: 50% below 10km while for altitudes above 10km those limits change to: Threshold accuracy: 100%; Target accuracy: 35%; Optimal accuracy: 20%. Namely, below 10 km, the target accuracy of 100 % is obtained whereas above 10km the optimal accuracy of 50% is achieved for the EUMETSAT NRT_PPF_v6.3 IASI/MetopA products.

1. INTRODUCTION

The main aim of this report is to validate the IASI/MetopA BRESCIA_v201510 volcanic SO_2 product. As the EUMETSAT demonstrational operational product only covers a few months at time of writing (June 2017 to October 2017), the ULB-LATMOS offline product (covering the period 2007-2013) will be employed to perform comparisons against collocated ground-based instruments and satellite observations. The report will briefly present the IASI/MetopA instrument, described the retrieval algorithm as was applied to the LATMOS and EUMETSAT facilities, compare the demonstrational product to the offline dataset, provide a short literature review of the various IASI SO_2 products and proceed in comparing them against Brewer and MAXDOAS spectrophotometer ground-based stations as well as OMI/Aura & GOME2/MetopA & MetopB observations.

1.1 THE IASI/METOPA INSTRUMENT

The IASI instrument, on board EUMETSAT's MetopA & MetopB satellites, is extensively described in Clerbaux et al., 2009. IASI is a Fourier Transfer Spectrometer associated with an imager designed to observe the thermal IR part of the spectrum emitted by the Earth-Atmosphere system in nadir-view. In Table 1 the main characteristics of the MetopA & MetoB buses and the IASI instrument are reproduced from Clerbaux et al., 2009.

Table 1. The main characteristics of the MetopA & MetopB satellites and the IASI instrument.

Metop A	Launched on October 19, 2006
Metop B	**Launched on September 17, 2012**
Altitude	~817 km
Orbit	Polar sun-synchronous
Inclination	98.7° to the equator
Local time	~09:30, descending orbit
Time for one orbit	101 min
Repeat cycle	29 days (412 orbits)
IASI	**Fourier transform spectrometer**
Size and weight	$1.7\,m^3$, 236 kg
Spectral range	645 to 2760 cm^{-1}
Spectral resolution	0.3–0.5 cm^{-1} (0.5 cm^{-1} apodized)
Radiometric noise	<0.1–0.2 K (650–1750 cm^{-1})
Scan type	Step and dwell
Field of view	50 km (3.33°) at nadir, with 4 simultaneous pixels of 12 km
Global Earth coverage	2 times per day
Full swath width	~2200 km (±48.3°), 120 pixels

1.2 THE IASI/METOPA SO₂ OFL AERIS AND IASI/METOPA & /METOPB NRT_PPF_V6.3 DATASETS[1]

Before moving forward with the validation, a section describing the inter-comparability of the BRESCIA v201510 algorithm as applied for the ULB-LATMOS off line product, hereafter IASI OFL AERIS, and the EUMETSAT operational product, hereafter IASI NRT_PPF_v6.3 is provided for completeness sake. In short, all IASI/A data discussed in this report for the period 2007-2013 were provided by the IASI OFL AERIS dataset and any IASI/A & IASI/B data for the period June 2017 to October 2017 were provided by the IASI NRT_PPF_v6.3 dataset. For details into the BRESCIA algorithm please refer to the Algorithm Theoretical Basis Document, hereafter ATBD, as well as the Product User Manual, hereafter PUM, documents.

i. The IASI/MetopA 2007 to 2013 IASI OFL AERIS SO₂ columns were downloaded from the ESPRI Data Centre of the French Atmosphere Infrastructure AERIS[2] and are fully described in Clarisse et al., 2012. In the aforementioned paper, a novel algorithm for the sounding of volcanic SO₂ plume above ∼5 km altitude was presented and applied to IASI. The algorithm is able to view a wide variety of total column ranges (from 0.5 to 5000 D.U.), exhibits a low theoretical uncertainty (3–5 %) and near real time applicability and was thence demonstrated on the recent eruptions of Sarychev in Russia, Kasatochi in Alaska, Grimsvotn in Iceland, Puyehue-Cordon Caulle in Chile and Nabro in Eritrea. A validation of this algorithm on the Nabro eruption observations using forward trajectories and CALIOP coincident measurements is presented in Clarisse et al., 2014.

ii. Since 20 June 2017 the IASI SO₂ Brescia algorithm data are included as demonstrational product in the NRT EUMETCAT dissemination channel, within the L2 PPF v6.3 BUFR dataset (https://www.eumetsat.int/website/home/News/DAT_3423485.html?lang=EN&pState=1). A description of the product can be found in the PUM. These IASI NRT_PPF_v6.3 data are provided both for IASI-A and IASI-B. Data have been processed from 20 June 2017 until 31 October 2017 and only non-trivial data has been extracted from the BUFR files on a global scale. The product provides SO₂ columns [in D.U.] at 5 assumed SO₂ cloud altitudes (7, 10, 13, 16 or 25 km). The BUFR files are converted to h5 files containing the non-empty values once per week at BIRA-IASB. The software used to read the BUFR files is ECMWF's publicly available ECCODES software package, through its python interface. The BUFR element tables files and sequence definitions for use with ECCODES that allow reading of the IASI BUFR data as obtained from the EUMETSAT BUFR definitions located at https://www.eumetsat.int/website/wcm/idc/idcplg?IdcService=GET_FILE&dDocName=ZIP_IASI_SO2_BUFR_TABLES&RevisionSelectionMethod=LatestReleased&Rendition=Web. The software preserves the information on the SO₂ quality flags such that filtering is possible afterwards.

As a short summary into the pertinent algorithm details we note that the IASI SO₂ total columns are calculated using brightness temperature differences and look up tables assuming different plumes heights. When the IASI L2 pressure (P), water vapor (H) and temperature (T) profiles are not available or when the SO₂ brightness temperature difference (BTD) is above 5K, the original off line algorithm associates with each observation P,T and H profiles by interpolating neighboring L2 profiles. The resulting IASI L2 profiles are then used for the SO₂ columns calculations. The criterion on the brightness temperature difference was introduced, as historically the quality of the IASI L2 meteorological data was sometimes found to be very poor in the center of dense volcanic plumes. Therefore, pixels with a BTD

---

[1] This section was co-authored by Maya George and Lieven Clarisse.
[2] http://iasi.aeris-data.fr/SO2/

above 5K are treated the same as those without L2. Recent versions (v6 and beyond) of the IASI L2 data have until now not shown any artefacts in the center of volcanic plumes. For this reason the IASI L2 data, if available, is always used in the Eumetsat operational product. Because of the operational set-up of the Eumetsat product (ie NRT processing, where neighboring pixels ahead of the track are not available), the pixels for which the IASI L2 data are missing are processed differently and ECMWF forecasts (3h, interpolated in time and space) data are used instead.

The ULB-LATMOS team performed comparison exercises with the EUMETSAT team during the set-up of the chain at the EUMETSAT facilities, hence transferring the BRESCIA algorithm from LATMOS to EUMETSAT. We present three major test cases in the following: the Sarychev, Russia, eruption for the 12th of June 2009, the Puyehue, Chile, eruption for the 6th of June 2011 and Bogoslov, Alaska, for the 8th of March 2017. We used the filtering criteria detailed in Section 5.2.2 of the Product User Manual: in the neighborhood of pixels with BTD >1, one can further consider pixels with BTD >0.4. All pixels that fit these criteria for one particular day were included in the comparison. Since we are comparing two IASI retrieval products, the collocation is perfect (i.e. no difference in time or space in the comparison).

The first two historical test cases, namely Sarychev in June 2009 and Puyuhue in June 2011, demonstrate that there is overall excellent agreement, especially for the larger altitudes, as can been seen from Figure 1-1 to Figure 1-4 inclusive. Table 2 summarizes the biases and standard deviations (note that the bias is calculated as OFL Aeris minus NRT_PPF_v6.3).This is logical, as the variability, and hence the errors of the P,H and T profiles are larger for lower altitudes. This is true for both the ECMWF profiles and the IASI L2 profiles. For altitudes above 7 km, the biases are below 0.3 DU (in absolute values) and the standard deviations below 0.8 DU, which is close to the detection threshold of the algorithm. At 7 km the largest differences are observed for the evening overpasses with a bias of -2.6 for Sarychev and a standard deviation of 3.3 for both Sarychev and Puyuhue. These numbers are well within the expected uncertainties for retrievals at this altitude. Note that the main uncertainty term of the retrieval is exactly the uncertainties in the L2 data. For a few observations, and again at lower altitude, very large differences are observed; e.g. for one particular pixel a difference of around 60 D.U. is observed. Such pixels are caused by retrievals with a thermal contrast (temperature difference between the baseline and the layer altitude) close to zero. Small difference in the temperature of the layer for such cases can have a very large effect on the retrieved column. As before, such retrievals already have a huge intrinsic uncertainty and for these the accuracy of the SO_2 product is very dependent on accurate L2.

Table 2 Biases (standard deviations) in D.U. for the two historical test cases.

	Sarychev AM	**Sarychev PM**	**Puyuhue AM**	**Puyuhue PM**
7 km	+0.3 (1.5)	-2.6 (3.3)	+0.7 (1.7)	+0.8 (3.3)
10 km	+0.3 (0.8)	+0.1 (0.7)	+0.0 (0.2)	+0.3 (0.6)
13 km	+0.3 (0.4)	+0.3 (0.3)	-0.1 (0.2)	-0.1 (0.1)
16 km	-0.1 (0.3)	-0.2 (0.5)	-0.1 (0.4)	-0.1 (0.2)
25 km	+0.1 (0.1)	+0.0 (0.2)	+0.0 (0.2)	+0.1 (0.1)

Sarychev 20090612 AM
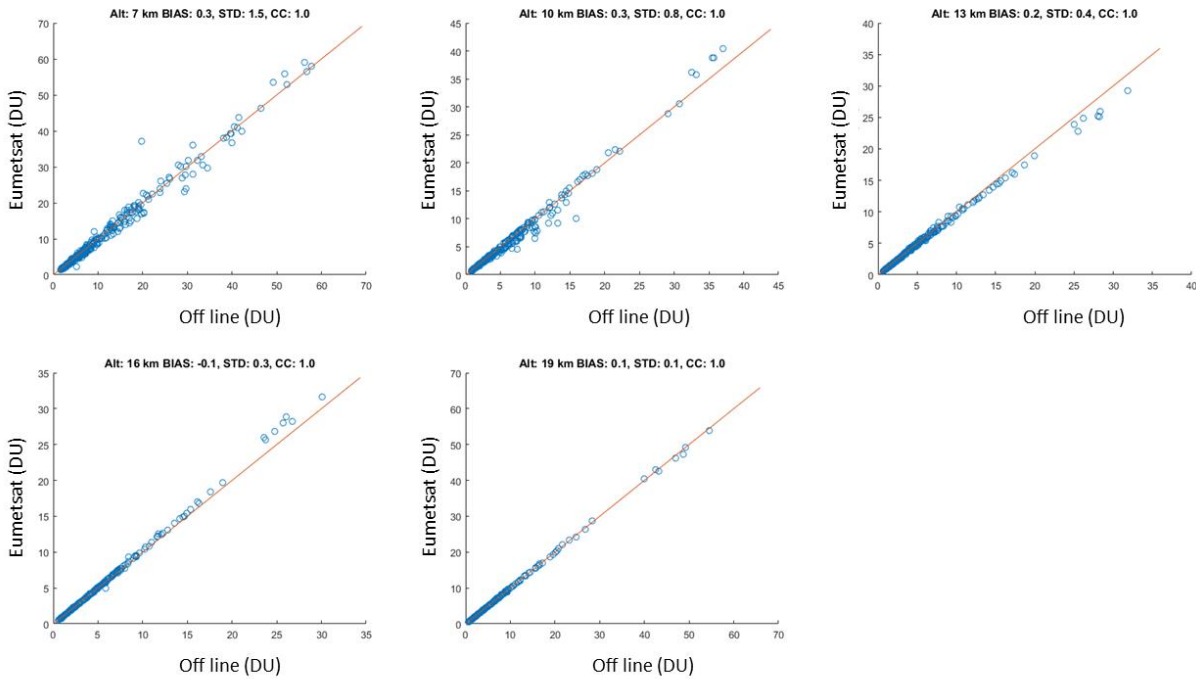
Figure 1-1. Comparisons between the Eumetsat NRT_PPF_v6.3 data and the OFL AERIS data, the 12th of June 2009, during the Sarychev eruption for the AM data. Biases and STD are expressed in DU. CC stands for correlation coefficient (1 for every assumed altitude of the plume). When bias<0, Eumetsat NRT>OFL.

Sarychev 20090612 PM
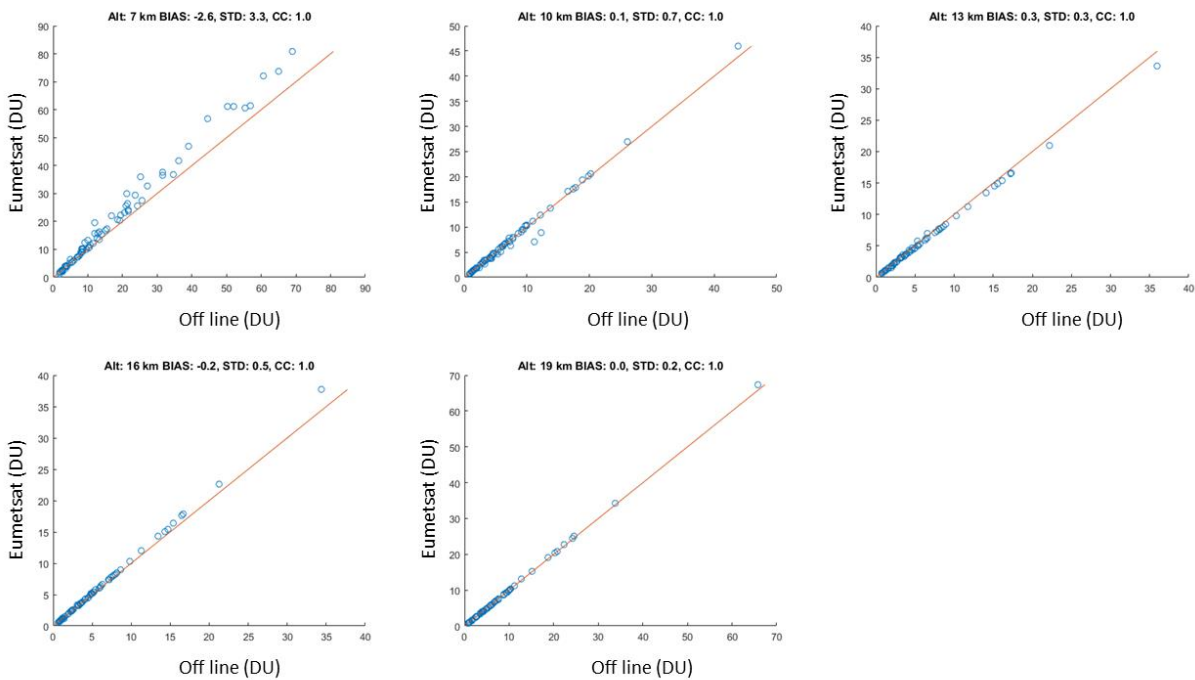
Figure 1-2. Comparisons between the Eumetsat NRT_PPF_v6.3 data and the OFL AERIS data, the 12th of June 2009, during the Sarychev eruption for the PM data. Biases and STD are expressed in DU. CC stands for correlation coefficient (1 for every assumed altitude of the plume). When bias<0, Eumetsat NRT>OFL.

Puyehue 20110612 AM
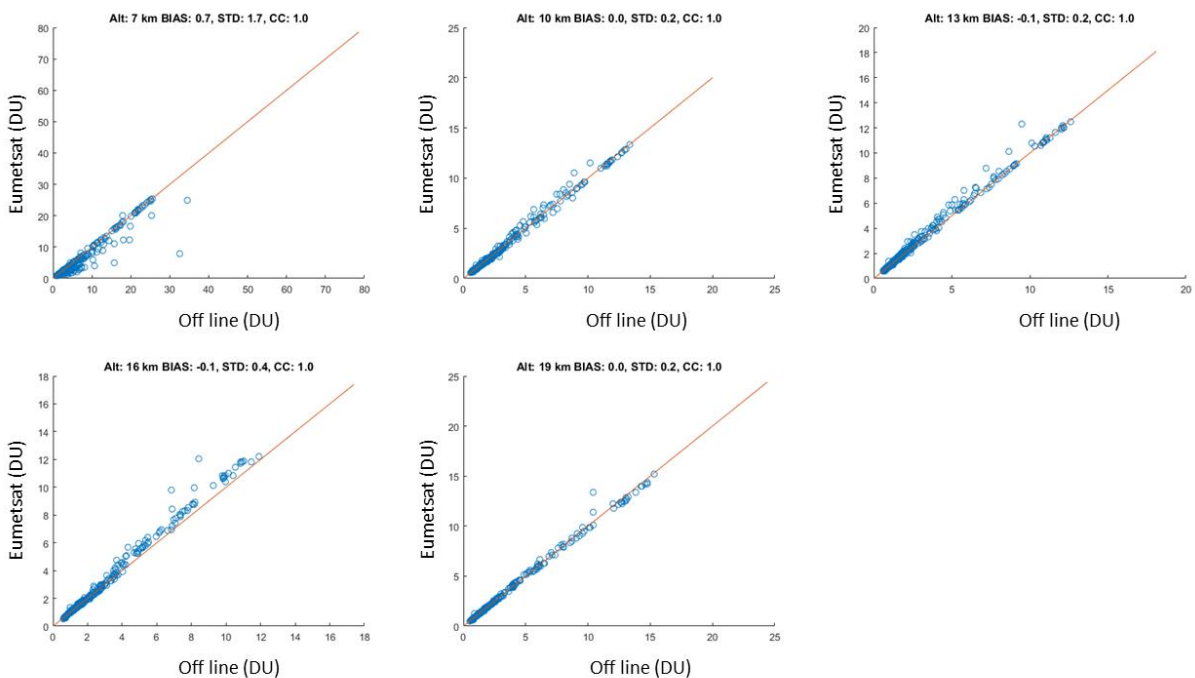
Figure 1-3. Comparison between the Eumetsat NRT_PPF_v6.3 data and the OFL AERIS data, the 6th of June 2011, during the Puyehue eruption for the AM data. Biases and STD are expressed in DU. CC stands for correlation coefficient (1 for every assumed altitude of the plume). When bias<0, Eumetsat NRT>OFL.

Puyehue 20110612 PM
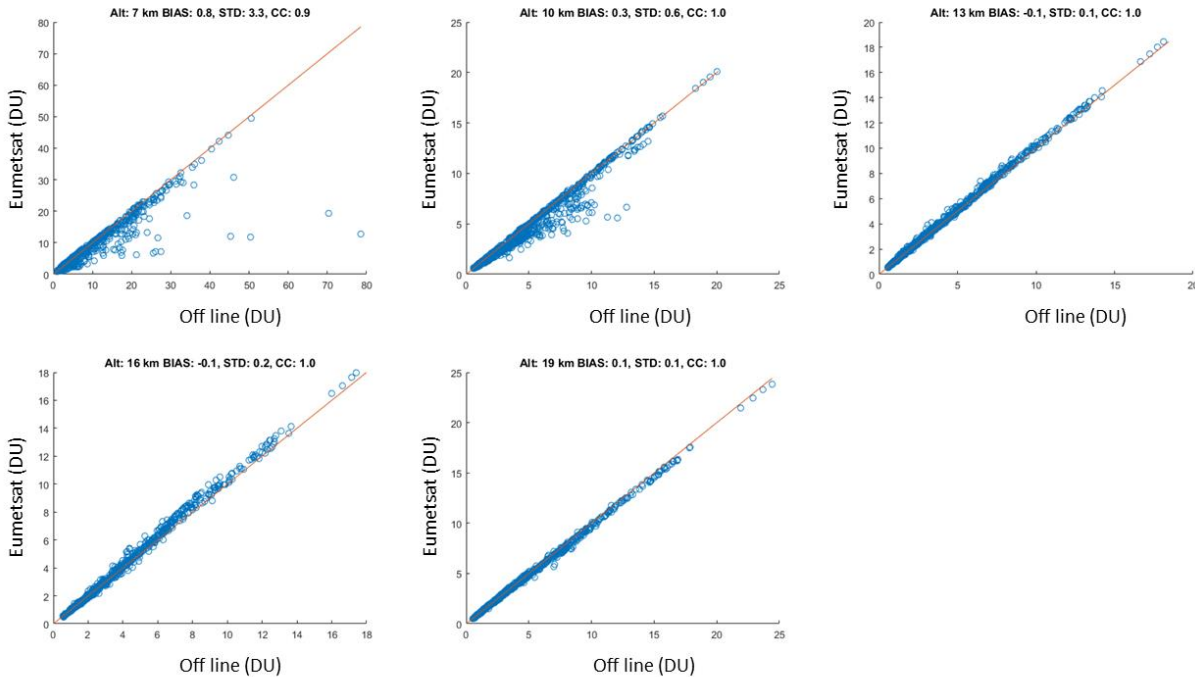
Figure 1-4. Comparison between the Eumetsat NRT_PPF_v6.3 data and the OFL AERIS data, the 6th of June 2011, during the Puyehue eruption for the PM data. Biases and STD are expressed in DU. CC stands for correlation coefficient (1 for every assumed altitude of the plume). When bias<0, Eumetsat NRT>OFL.

The third test case, that of the Bogoslov eruption of the 8th of March 2017, provides SO_2 columns only for AM data. For this comparison, we discriminate the pixels where IASI L2 are available (QFLAG=9, flag available in the NRT data) and pixels where IASI L2 are not available and replaced by forecasts data (QFLAG=11, flag available in the NRT data) in the Eumetsat NRT_PPF_v6.3 product. Note that the when QFLAG=9, the L2 data that is used is only identical for those pixels where the SO_2 brightness temperature is smaller than 5K. See section 5.2.1 of the PUM for the QFLAG definitions.

In Figure 1-5 and Figure 1-6, OFL product uses interpolation when L2 is missing or SO_2 brightness temperatures larger than 5K, NRT product uses forecasts when IASI L2 are missing. As is expected, for the lower columns (corresponding to a DBT below 5K), the two datasets agree perfectly. Above the differences are similar to the previous test cases.
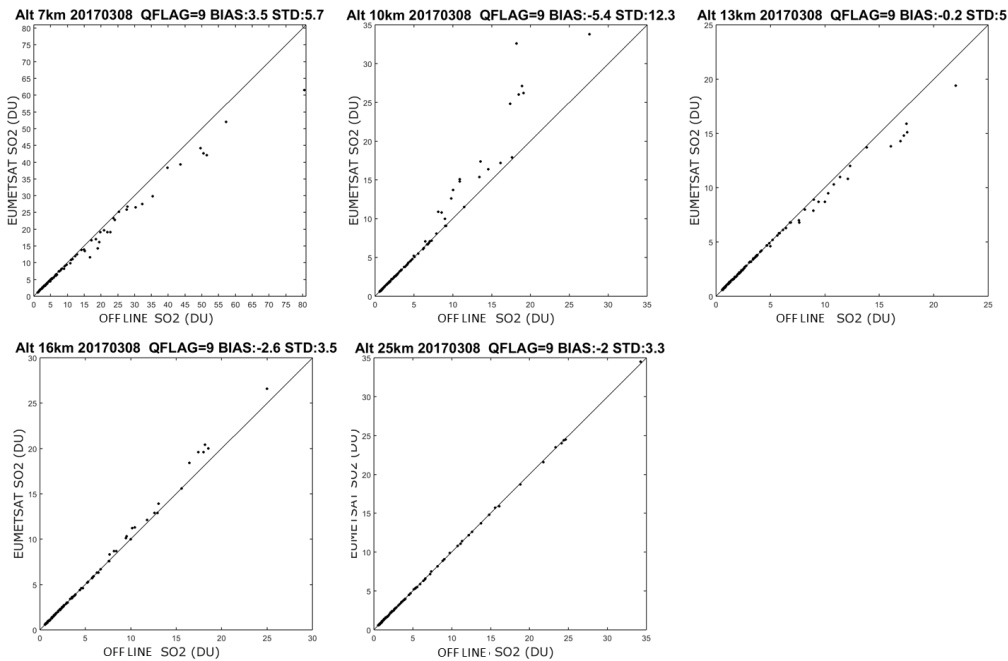
Figure 1-5. Comparison between the Eumetsat NRT_PPF_v6.3 data and the OFL AERIS data, the 8th of March 2017, in Alaska, AM data, for QFLAG=9 data (IASI L2 available). Unlike the previous plots, biases and SDT are expressed in percentage. When bias<0, Eumetsat NRT>OFL.
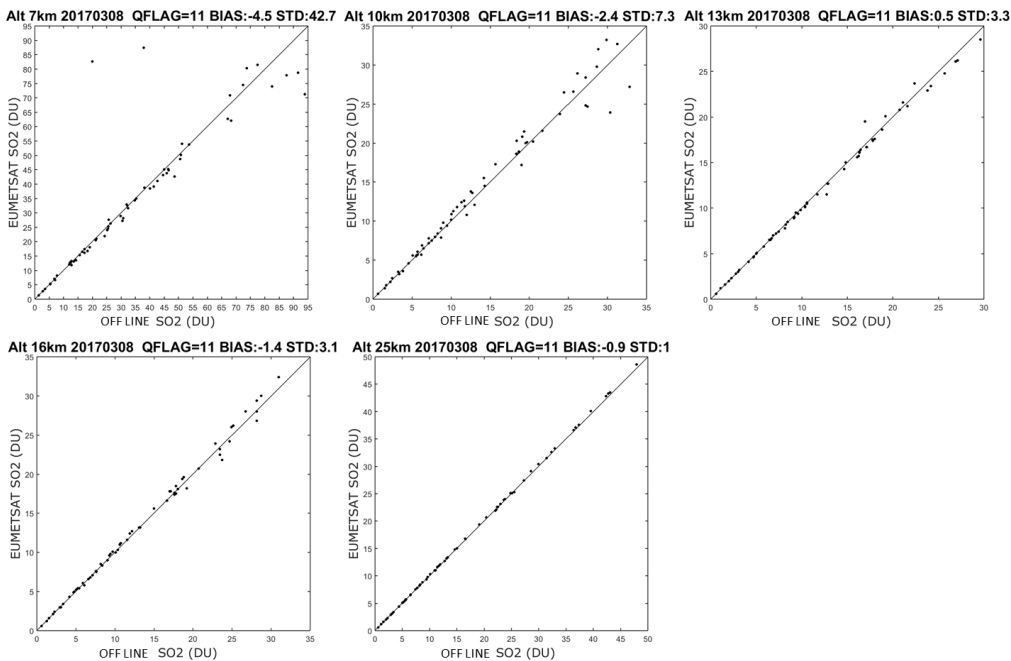
Figure 1-6. Comparison between the Eumetsat NRT_PPF_v6.3 data and the OFL AERIS data, the 8th of March 2017, in Alaska, AM data, for QFLAG=11 data (IASI L2 non available). Unlike the previous plots, biases and SDT are expressed in percentage. When bias<0, Eumetsat NRT>OFL.
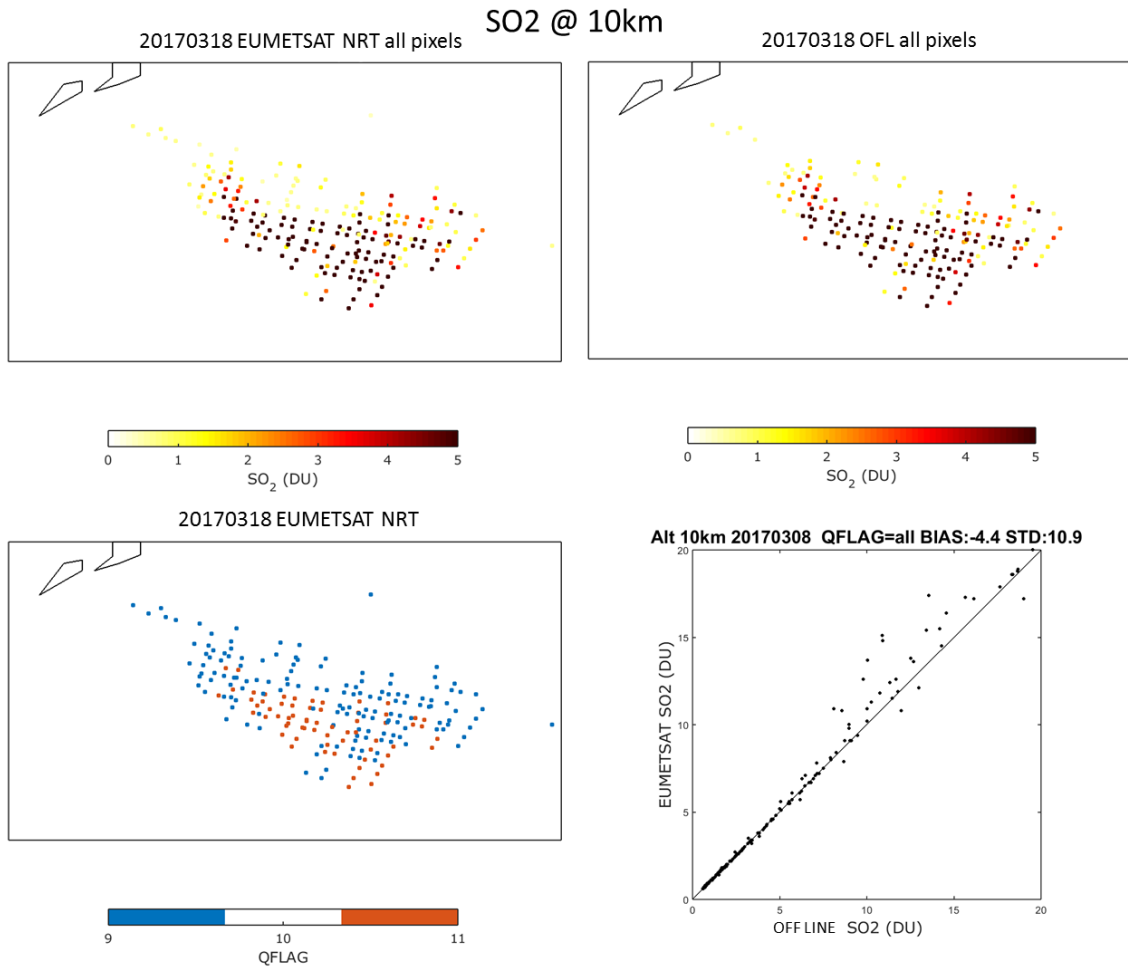
Figure 1-7. Same Alaska case presented in Figure 1-5 and Figure 1-6 but with a focus on data with the assumed altitude plume at 10 km. All pixels (QFLAG 9 and 11) are plotted.

We hence show that the ULB-LATMOS OFL AERIS data product is in excellent agreement with the EUMETSAT NRT_PPF_v6.3 product, which was made operationally available to the validation teams since June 20th 2017. For the Sarychev case, biases are between -2.6 (STD 3.3) and 0.3 (STD 1.5) DU. For the Puyehue case, biases are between -0.1 (STD 0.4) and 0.8 (STD 3.3) DU. For the Alaska case, biases are between -5.4 (STD 12.3) and 3.5 (STD 5.7) % when QFLAG=9, i.e. when both products are using the same IASI L2 data. When QFLAG=11 (Eumetsat NRT_PPF_v6.3 product uses forecasts and OFL AERIS uses interpolation), biases are between -4.5 (STD 42.7) and 0.5 (STD 3.3) %.

1.3 IASI SO₂ COLUMNS THROUGH A SHORT LITERATURE REVIEW

From the beginning of the IASI/MetopA mission the SO_2 retrieval was in the front-line of scientific endeavours; in Clarisse et al., 2008, the first test-case for the retrieval of SO_2 plume was attempted on a moderate eruption of Jebel at Tair, a stratovolcano located in the Red Sea between Yemen and Eritrea whereas in Karagulian et al., 2010, the 2008 Kasatochi eruption was examined. Athanassiadou et al., 2016, also analysed IASI observations over three volcanic eruptions, Mount Sinabung and Kelut, Indonesia and Bárðarbunga in Iceland based on the Clarisse et al., 2008, methodology, adapted. This latter eruption was also extensively discussed in Schmidt et al., 2015, who showed how the 2014–2015 Bárðarbunga-Veiðivötn fissure eruption transported volcanic SO_2 in the lowermost European troposphere over long distances and detected by air quality monitoring stations up to 2750 km away from the source.

IASI data have also been used in comparative studies such as the work of Theys et al., 2013, where SO_2 observations by high spectral resolution satellite instruments operating both in the ultraviolet-visible (OMI/Aura and GOME-2/MetOp-A) and thermal infrared (IASI/MetOp-A) spectral ranges, and multispectral satellite instruments operating in the thermal infrared (MODIS/Terra-Aqua), were shown to agree well and be able to track, in tandem, the spatiotemporal evolution of volcanic plumes. In Theys et al., 2015a, the IASI dataset was used as validation tool for a new OMI/Aura SO_2 algorithm whereas in Zerefos et al., 2017, the IASI data was exploited in examining the adequacy of the existing Brewer spectrophotometer network to supplement other ground-based networks and space-born instruments to detect SO_2 plumes of volcanic origin.

Lately, great efforts have been made to tune the standard IASI algorithm in order to sense anthropogenic, near-surface sources of SO_2. In Boynard et al., 2014, boundary layer SO_2 from the very much polluted North China Plain was demonstrated by IASI whereas Bauduin et al., 2014, using the same dedicated algorithm, successfully obtained and validated four years of measurements around the similarly polluted Russian city of Norilsk in the Arctic Circle. In the very recent work of Bauduin et al., 2016, a global catalogue of lower tropospheric SO_2 sources has been achieved whereupon continuously emitting locations were identified in full: industrial and power plant emissions in China, South Africa, Bulgaria and Turkey, smelter emissions in Northern Russia and Kazakhstan, continuously outgassing volcanoes such as Mt Etna in Italy, Popocatepetl in Mexico, Nyiragongo in D.R. of Congo, oil refineries in Iran, and so on.

Furthermore, within AC SAF CDOP-3, the actual plume altitude will be retrieved. The IASI instrument, as discussed above, can easily detect the SO_2 signature in case of volcanic eruption, see the Support to Aviation Control Service, http://sacs.aeronomie.be/. Plumes can be followed during both day and night using the IASI data, but a crucial bit of missing information is the altitude level of the plume, a vital parameter for aircraft safety. The IASI spectrally resolved channels can be used to derive SO_2 height, with an accuracy of about 2 km using a specific formalism described in Clarisse et al., 2014 and has already been validated with Calipso data.

In the present report, we focus on volcanic SO_2. A list of the highest emitting volcanoes for the decade 2005 to 2014 are presented in Appendix I. in Table 7 for quick reference [see also Fioletov et al., 2016.]

2. IASI/MᴇᴛᴏᴘA OFL AERIS ᴄᴏᴍᴘᴀʀɪsᴏɴs ᴀɢᴀɪɴsᴛ ᴛʜᴇ Bʀᴇᴡᴇʀ SPECTROPHOTOMETER NETWORK

2.1 Tʜᴇ Bʀᴇᴡᴇʀ Sᴘᴇᴄᴛʀᴏᴘʜᴏᴛᴏᴍᴇᴛᴇʀ SO₂ ᴅᴀᴛᴀsᴇᴛ

The Brewer spectrophotometer is a fully automated, diffraction-grating ground-based instrument that observes the near UV solar intensity. The spectrophotometer measures the intensity of radiation in the ozone ultraviolet absorption spectrum at five wavelengths (306.3 nm, 310.1 nm, 313.5 nm, 316.8 nm and 320.1 nm) with a resolution of 0.6 nm which enables the extraction of both total ozone and sulphur dioxide columns (Kerr et al., 1980). About a hundred Brewer spectrophotometers contribute high-precision ozone data to the World Ozone and UV Radiation Data Center, http://woudc.org/home.php, from 1995 onwards. The existing Brewer network also reports SO_2 columnar measurements as well, which can be used for scientific analysis but with great caution. The signal-to-noise ratio for the SO_2 absorption is usually quite low and therefore well calibrated instruments are required to monitor SO_2 columnar amounts (Kerr et al., 2010; Koukouli et al., 2014). Details on the method with which SO_2 is measured by the Brewer spectrophotometer can be found in Kerr et al., 1988, and De Backer and De Muer, 1991. According to Fioletov et al., 2016, the uncertainty of the Brewer direct sun SO_2 measurements is about 1 D.U. and is typically insufficient for air quality applications. Although the Brewer instrument has difficulties in detecting low columnar SO_2 concentrations, in extreme cases, such as volcanic eruptions, the SO_2 levels typically rise well above the instrumental noise and can be identified with the Brewer instrument as shown in Fioletov et al., 1998 and Zerefos et al., 2017. In the latter work, during the 2008 Kasatoschi eruptive period, the mean SO_2 column departures from the unperturbed 10-day pre-volcanic baseline measured by Brewers, two OMI/Aura NASA columns[3] and GOME-2/MetopA GDP4.7 data[4] over Europe, Canada and the USA showed promising findings, as per their Figure 14 reproduced here as Figure 2-1.

---

[3] https://avdc.gsfc.nasa.gov/index.php?site=1442350108
[4] http://o3msaf.fmi.fi/index.html
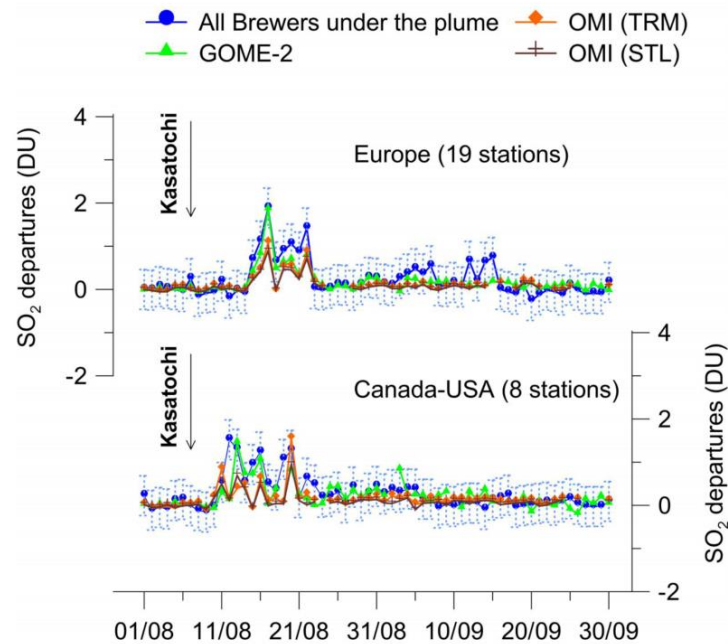
Figure 2-1. Mean SO₂ column departures from the unperturbed 10-day pre-volcanic baseline measured by Brewers, two OMI/Aura NASA columns (TRM, STL) and GOME-2/MetopA GDP4.7 data during August–September 2008 over Europe and Canada and the USA following the 2008 Kasatochi volcanic eruption. The arrow marks the date of the eruption (7 August 2008). Image courtesy of Zerefos et al., 2017, Fig. 14.
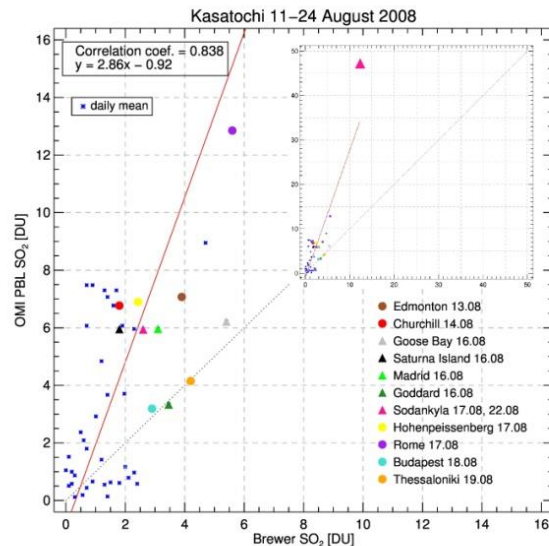
Figure 2-2. Scatter diagram of OMI/Aura NASA PBL SO₂ column measurements versus the daily SO₂ column measured from Brewer spectrometers during the effective period of Kasatochi eruption. Different colors represent different stations for specific days. In PBL case, the inside scatter diagram shows the actual axis range. Image courtesy of Theofanis Stamoulis, M.Sc.thesis, Fig 3.9, 2016.

For the same eruptive period, the scatter diagram of OMI/Aura NASA PBL SO_2 column measurements versus the daily SO_2 column measured from Brewer spectrometers also provided a moderate correlation of 0.84, discussed in the work of Stamoulis, 2016, Fig. 3.9, reproduced here as Figure 2-2.

The Brewer SO_2 data reported in WOUDC have been used in previous IASI SO_2 studies as well but frugally; in Carboni et al., 2016, the April and May 2010 ground-based observations over Europe were used for comparisons during the Eyjafjallajökull eruptive periods. With careful screening and cautious considerations, the scatter plot between the IASI observations and the Brewer collocation was found to be quite encouraging as shown in their Figure 5, reproduced in this report as Figure 2-3.
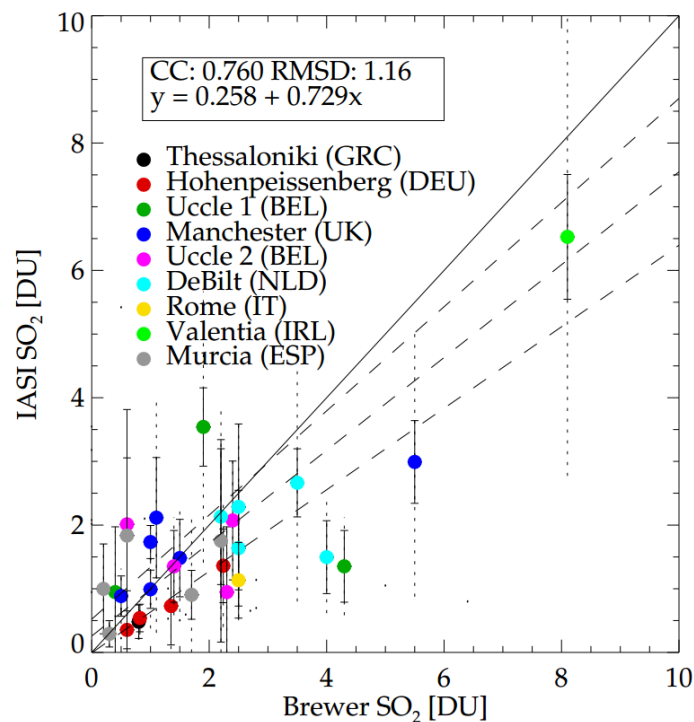
Figure 2-3. Scatter plot of IASI SO_2 measurements against collocated daily SO_2 column amounts measured by different European Brewer spectrometers. Image courtesy of Carboni et al., 2016, Fig. 5.

In this study we analyzed fifty four Brewer stations that reported SO_2 columns in the WOUDC repository on a global scale. Those are enumerated in APPENDIX II., out of which thirty six provide collocations with the IASI overpasses at a 50km search radius [no temporal criterion]. Due to the small amount of collocations, the data were grouped by geographic criteria: Europe, Asia, North America, South America, Middle East & Russia. However, from the South American stations only a handful of collocation pass the quality assurance criteria, hence no comparisons may be shown for that part of the Globe.

Europe

y=3.11+0.32x

- Budapest
- Thessaloniki
- Sodankyla
- Sondrestrom
- Rome University
- Madrid
- De Bilt
- Valentia
- Poprad Gavonce
- Murcia
- Manchester
- Reading
- La Coruna
- Zaragoza
- Uccle
- Hohenpeissenberg

Europe

IASI
Brewer

Asia

y=3.78+0.01x

- NewDelhi
- Poona
- Seoul
- Chengkung
- Longfengshan
- Pohang
- Bandung
- Taipei

Asia

IASI
Brewer

Middle East & Russia

y=1.77+0.32x

- Kislovodsk
- Obninsk
- Ankara
- Tomsk

Middle East & Russia

IASI
Brewer

Figure 2-4. Comparisons for all possible collocations between Brewer spectrophotometer reported SO_2 column and IASI OFL AERIS overpasses for the time period 2007 to 2013. Left column: scatter plots between IASI SO_2 [y-axis] and Brewer SO_2 [x-axis] with the different stations within each geographic region are coloured differently. Right column: time series of the columns for the year 2008, possibly affected by the Kasatoschi eruption. From top to bottom: Europe, Asia, Middle East & Russia and North America collocations are shown.

In Figure 2-4, left column, the comparisons between IASI OFL AERIS and Brewer SO_2 columns for all possible collocations for the time period provided are grouped in geographical location; from top to bottom, Europe, Asia, Middle East & Russia and North America. In different colour, the specific stations that provide the collocations are provided. In the top left, the linear fit line is also shown. In general, the IASI data provide systematically larger columns with y-intercepts ranging between 2 and 4 D.U. In the right column, the time series for year 2008, the year of the Kasatochi eruption is shown. Notably, for Europe, Middle East & Russia and North America, collocations exist only for the eruptive period. However, in Asia [second row, right] significant SO_2 loadings are observed throughout the year which leads us to postulate that both instruments are sensing the high anthropogenic SO_2 contribution, well known for the region [see van der A, et al., 2017, and references therein.]

3. IASI/METOPA OFL AERIS COMPARISONS AGAINST THE MAXDOAS NETWORK[5]

In order to validate the IASI BRESCIA 201510 SO$_2$ products, several BIRA-IASB MAXDOAS stations were employed (http://uv-vis.aeronomie.be/groundbased/stations) which cover the available datasets time-period (2007-2013 and June, 20th 2017 onwards):

- **OHP** (44°N, 7.71°E, **France**) measured in MAXDOAS geometry from 2005 (Valks et al., 2011) to March 2017;

- **Jungfraujoch** (46.5°N, 7.98°E, **Switzerland**) is measuring in ZenithSky geometry since the '90 with a SAOZ and in MAXDOAS geometry since 2010 (Hendrick et al., 2012);

- **Harestua** (60.2°N, 10.75°E, **Norway**) is measuring in ZenithSky geometry since the '90 and with an updated instrument since November 2012 (Hendrick et al., 2007);

- **Uccle** (50.5°N, 4°E, **Belgium**) measured with a mini-MAXDOAS instrument from May 2011 to early 2016 (Gielen et al., 2014) and a new instrument has been installed end of January 2017;

- **Beijing** measured between 06/2008 to 04/2009 on the roof of IAP, in the city center and since 2010 in **Xianghe** (39.75°N, 116.96°E) with a MAXDOAS (Clémer et al., 2010; Hendrick et al., 2014);

- **Bujumbura** (3°S, 29°E, **Burundi**) is measuring since 11/2013 with a MAXDOAS (Gielen et al., 2017);

- **Reunion** (21°S, 55°E, **Reunion Island**) is measuring since April 2016 with a MAXDOAS.

IASI SO$_2$ data have been extracted in a radius of 150km around these 8 ground-based stations and the time-series of the IASI VCD data at 13km and 16km is presented in Figure 3-1 for the OFL Aeris product and in Figure 3-2 for the IASI-A and IASI-B NRT_PPF_v6.3 product. While the OFL Aeris product is pre-filtered, the NRT_PPF_v6.3 product is not, and once applying the recommended filter on the brightness temperature difference value suggested in the PUM (section 5.2.2), i.e. only looking at the retrievals in the neighbourhood of SO2_BT_DIFFERENCE>1K pixels, no significant volcanic event is detected around the BIRA MAXDOAS stations. In addition of the clear difference number of points and noise between figure 3-1 and 3-2, Figure 3-3 shows the first eruption that happened since the IASI NRT_PPF_v6.3 data are distributed: the 06/09/2017 Vanuatu eruption (visible during 3 consecutive days with IASI). The scatter points are color-coded as a function of the ΔBt value of each pixel: all of them (knowing that only ΔBt>0.4 are distributed), larger than 1K (in blue) and larger than 2.9K in red. 1K and 2.9K are chosen as the first is the recommended lower limit suggested in the PUM (section 5.2.2), and 2.9K is a value often used as a volcanic flag (i.e. in the SACS website, Table 3 of Brenot et al., 2014). Another enhanced SO$_2$ signal has been captured by the IASI NRT_PPF_v6.3 on the same region on 21 to 23 October 2017.

---

[5] This section was co-authored by Gaia Pinardi and colleagues from BIRA/IASB
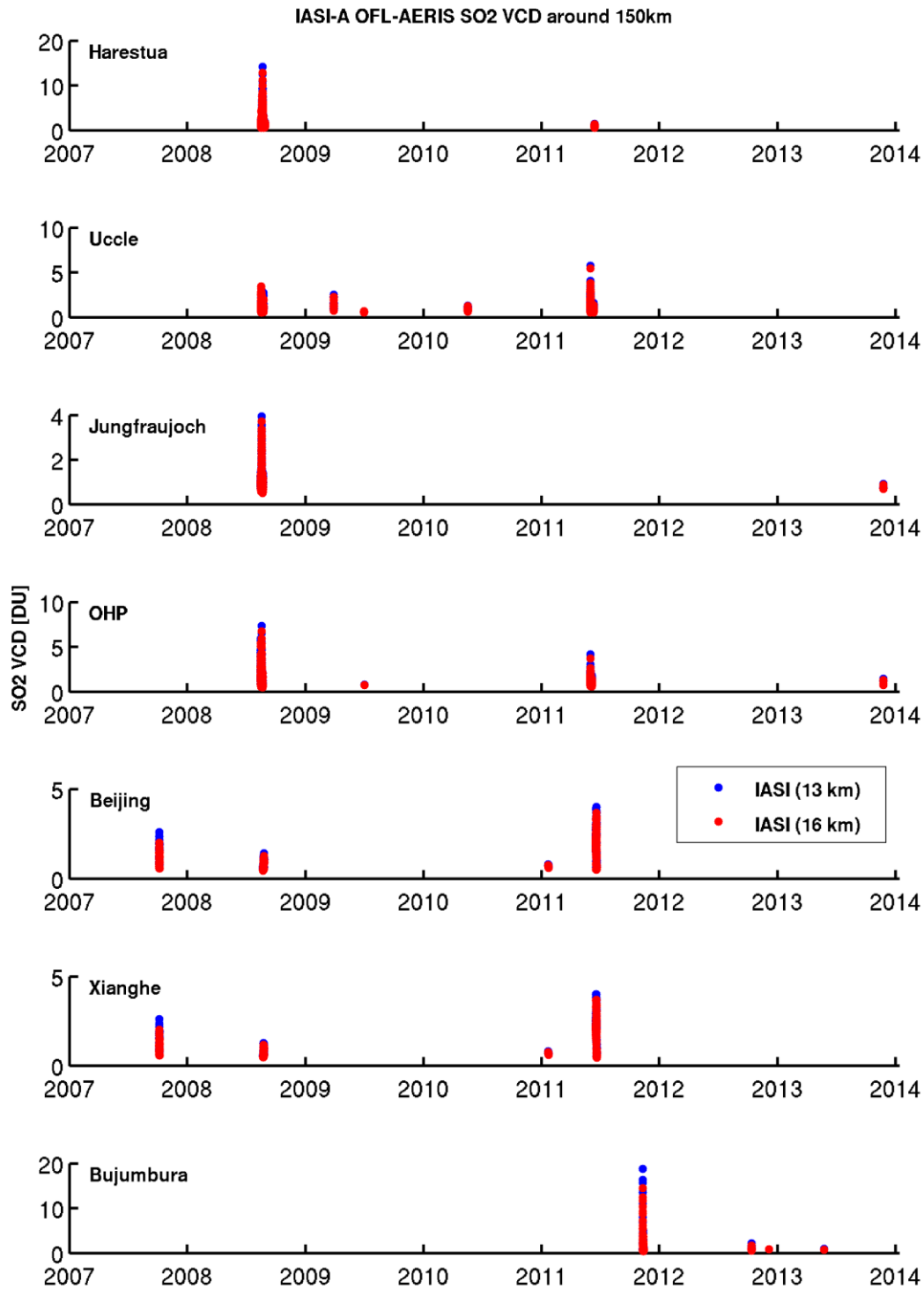
Figure 3-1. IASI SO₂ OFL-AERIS columns overpasses in a radius of 150km around the BIRA-IASB stations; 13km (blue dots) and 16km (red dots).
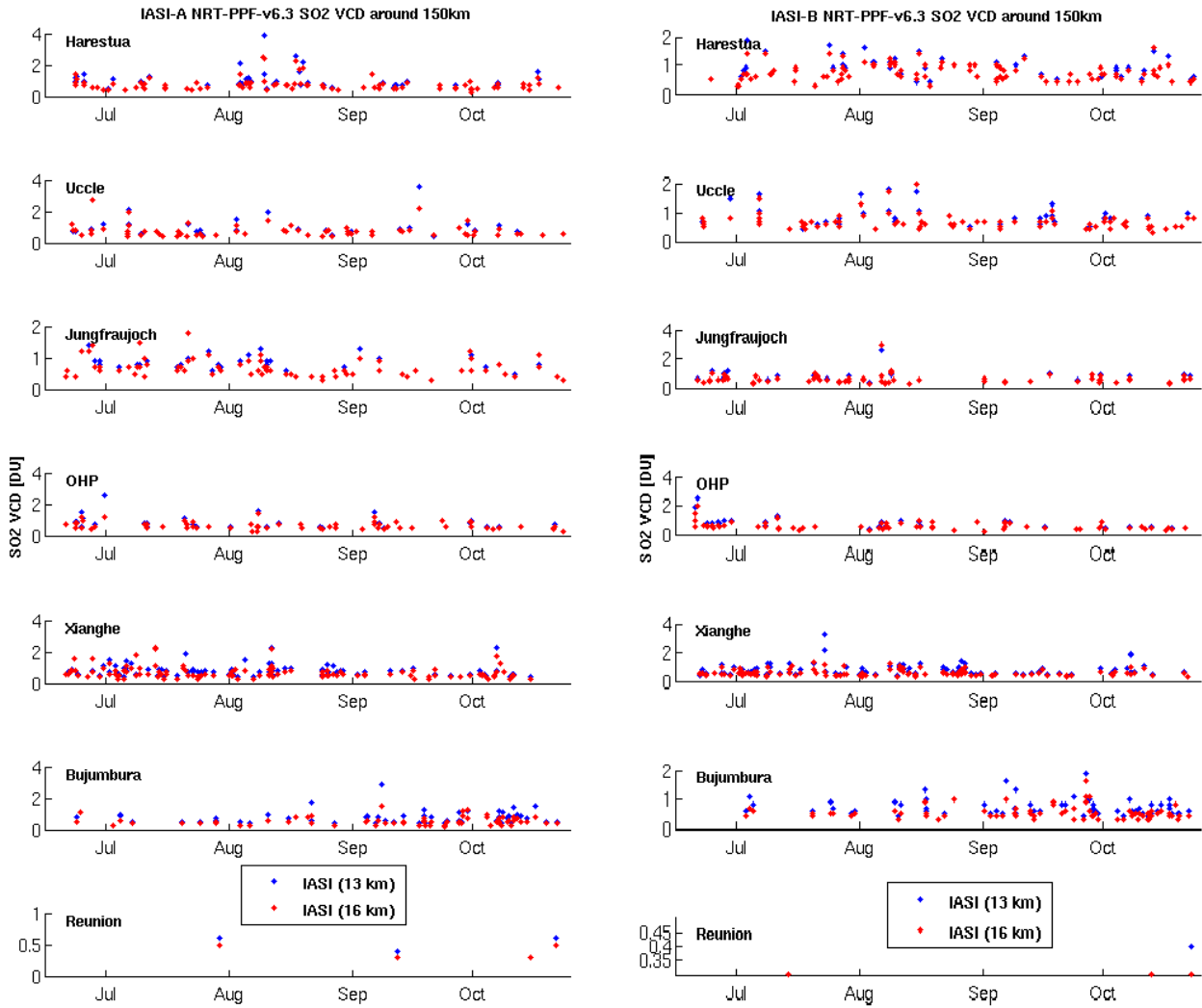
Figure 3-2. IASI SO$_2$ NRT-PPF-v6.3 VCD columns overpasses in a radius of 150km around the BIRA-IASB stations since 16 June 2017; 13km (blue dots) and 16km (red dots). MetopA on the left and MetopB on the right columns.
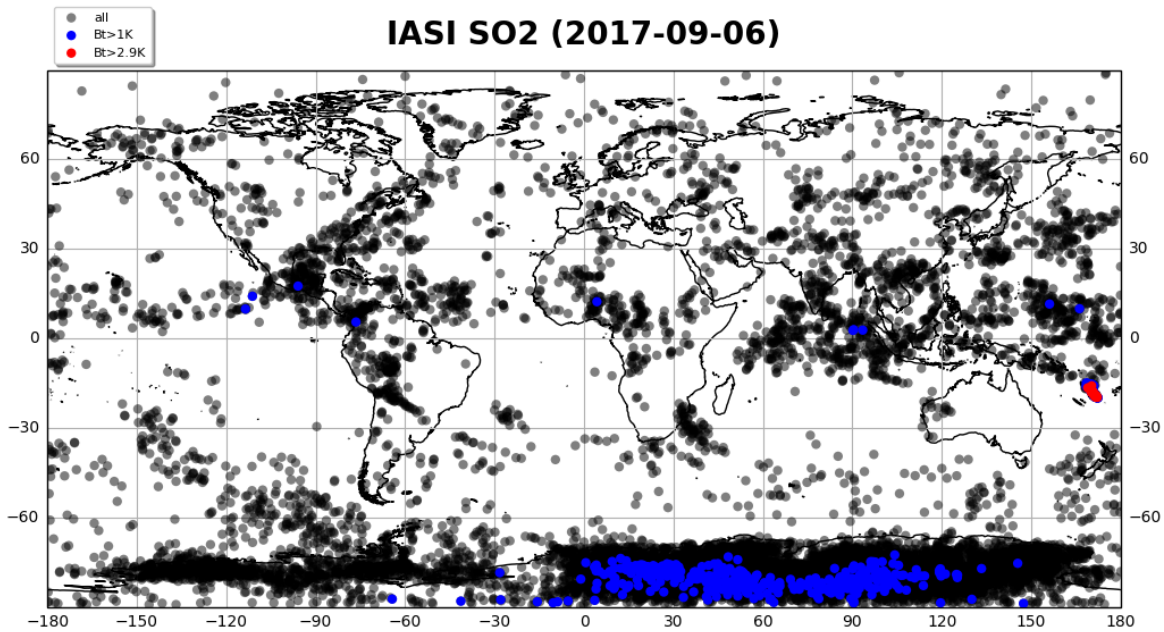
Figure 3-3. IASI SO$_2$ NRT_PPF_v6.3 pixels location for 06/09/2017, color-coded as a function of their ΔBt value.

In the OFL Aeris longer dataset, large stratospheric eruptions can be seen over most of the BIRA-IASB stations, such as the Kasatochi eruption of 7 August 2008 (Clarisse et al., 2012) or the Nabro eruption (12 to 28 June 2011, Clarisse et al., 2014), that travelled around the Northern hemisphere. Table 2 of Carn et al., 2016 and references therein have also been used to relate the SO$_2$ signal to known eruptions, for example, over Xianghe and Beijing in China, the Jebel al Tair plume is seen by IASI in October 2007, however the MAXDOAS instrument was not installed yet. The SACS website (http://sacs.aeronomie.be/, Brenot et al., 2014) is also a useful tool to recognize and follow the volcanic eruptions seen by IASI (and other satellites). For example in January 2011 a small signal (less than 1DU for the 13km and 16km SO$_2$ height and less than 2DU for the other SO$_2$ altitudes assumed for the column) is measured by IASI in a radius of 150km around the Xianghe and Beijing stations, but this signal could not be related to any volcanic plume (no alert on the SACS service for this region (n° 210): http://sacs.aeronomie.be/alert/Archive/index.php?Year=2011&Month=01&Day=02&InstruGOME2=0&I nstruOMI=0&InstruSCIA=0&InstruIASI=1&InstruAIRS=0&monthly=1) and will thus not be investigated further.

Unfortunately, the OHP instrument and the first version of the Harestua instrument are measuring in the spectral region from 323-390nm and are thus not covering the SO$_2$ analysis region (305-317.5nm). Moreover, the very small overlapping time-period between available OFL-AERIS IASI dataset (2007-2013) and the installation of the Bujumbura MAXDOAS (November 2013) also prevent to use this station for further investigations.

Considering the available IASI and ground-based measurements and discussion above, only 4 stations have an interesting eruption to look to. SO$_2$ analysis are not performed routinely, and only the time-periods specified in Table 3 have been analysed from the BIRA-IASB ground-instruments, in order to compare to IASI. The ground-based spectra have been analysed using the DOAS settings specified in Wang

et al., 2014 (analysis in the 305-317.5nm window) with a fixed reference spectrum close to the period of interest (on a day not affected by the eruption). The slant columns measured at zenith are used to estimate the stratospheric SO_2 content by using a geometrical stratospheric AMF that depends only on the solar zenith angle (Honninger et al., 2004):

$$AMF_{strato} = 1/cos(SZA) \tag{1}$$

For large stratospheric eruptions, such as Kasatochi, Grimsvotn, Nabro, etc. (Carn et al., 2016 and Hopfner et al., 2015), both MAXDOAS and ZenithSky instruments are sensitive to the SO_2 in the stratosphere, and the stratospheric SO_2 content is obtained as:

$$VCD_{strato} = DSCD_{zenith}/AMF_{strato} \tag{2}$$

Table 3. Ground-based periods analysed for comparisons between ground-based BIRA-IASB instruments and IASI OFL Aeris SO_2 columns.

Station [SACS region]	Period	Main eruption
Beijing [310]	01/08/2008 to 20/09/2009 rq: gap in the data between 22/08 and 14/09 included	Kasatochi
Xianghe [310]	June 2011	Nabro
Jungraujoch [106]	17/11/2013 to 30/11/2013	Etna (23/11/2013)
Uccle [106]	28/5/2011 to 15/6/2011	Grimsvotn (May, June 2011);

Beijing

For the Beijing measurements, the only common period is during the Kasatochi eruption, but unfortunately an instrumental issue prevented to perform measurements in the 22 August - 14 September 2008 period. A large peak of SO_2 is seen with the MAXDOAS on 21 August, just before the instrumental problem, while IASI probed the plume around Beijing in the following days, but no common measurement is available for a quantitative comparison.

Jungfraujoch

For the Jungfraujoch station, during the Kasatochi eruption only the BIRA SAOZ was measuring, which is not measuring in the SO_2 region. However, one eruption happened after the new MAXDOAS instrument was installed, in November 2013. Figure 3- shows the time-series of the MAXDOAS VCD obtained from the zenith measurement and applying a stratospheric AMF during the second half of November 2013. The IASI VCD data for SO_2 loading between 10 and 16km height are also reported, and show very coherent SO_2 amounts. Using SACS website, the SO_2 plume can clearly be identified as an Etna plume from an eruption on the 23th of November travelling first east and then north and reaching Jungfraujoch on the 24th. Poret et al. 2017 (http://meetingorganizer.copernicus.org/EGU2017/EGU2017-7635.pdf) estimated the plume height at about 10km. Focusing on the 24th November and the IASI OFL Aeris columns at 10km, Figure 3- show the very good agreement of about half a DU.
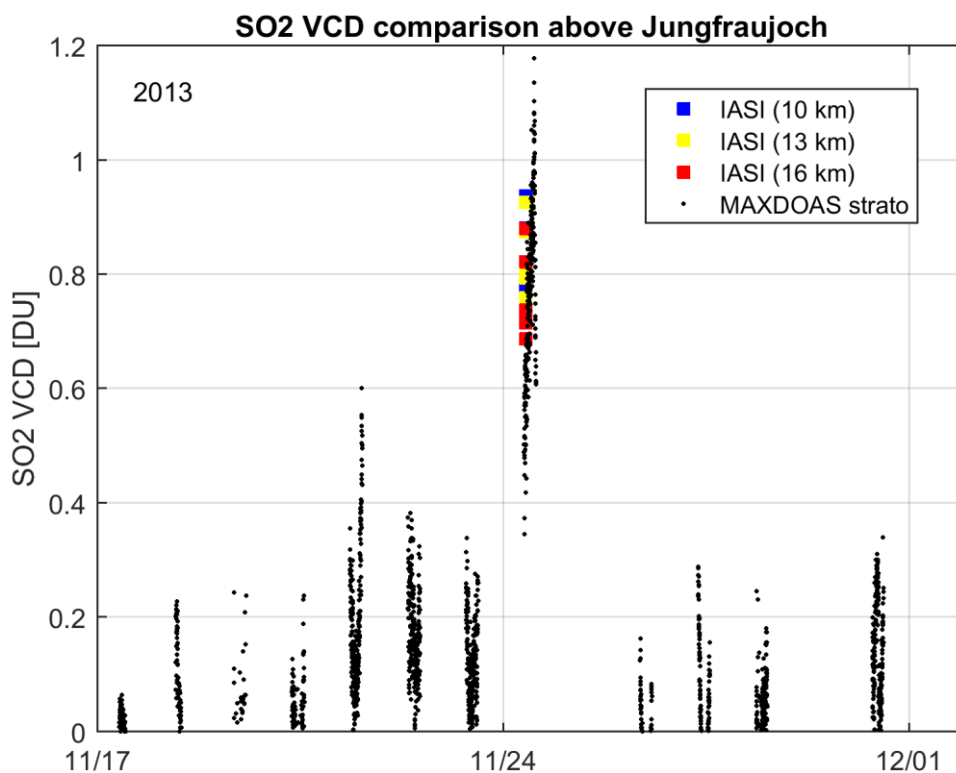
Figure 3-4. SO_2 VCD comparisons at Jungfraujoch focusing on the second half of November 2013. IASI columns overpasses in a radius of 150km around the stations are reported for 10km, 13km and 16km, and the MAXDOAS VCD are estimated from the zenith measurements with a fixed DOAS reference taken on 17/11/2013 at noon.
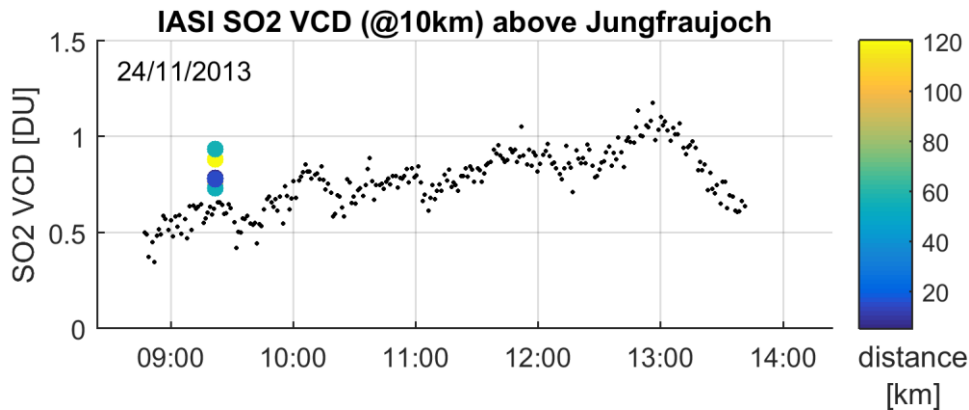
Figure 3-5. SO$_2$ VCD comparisons at Jungfraujoch focusing on the 24 November 2013. IASI OFL Aeris columns for an estimated SO$_2$ at 10km overpasses in a radius of 150km around the stations are color-coded as a function of the station distance.

Xianghe

The Xianghe station is more challenging because of the SO$_2$ pollution that is seen by the MAXDOAS instrument all year long (Wang et al., 2014), and that should be disentangled from the volcanic signal. To that end, several approaches have been tested, using the different geometries of measurement. This instrument is indeed measuring also in DirectSun mode allowing the retrieval of total SO$_2$ VCD while from the MAXDOAS profiling algorithm low tropospheric profiles and tropospheric SO$_2$ columns can be retrieved (Wang et al., 2014). These 2 datasets are shown in the upper panel of Figure 3-.

Most of the time, the total SO$_2$ from the DirectSun and the tropospheric SO$_2$ from the MAXDOAS profiling are very consistent, sign that most of the SO$_2$ are in the lowest layers, sensed by both techniques. Some days, however, the DirectSun signal is larger, sign of some additional (stratospheric) SO$_2$ content. The difference between the DirectSun and the MAXDOAS data are compared in the lower plot of Figure 3-.to the stratospheric VCD estimated from the zenith measurements using formula (2) as discussed before. For days where both datasets agree well, we are confident of the retrieved stratospheric SO$_2$, and this can be compared to IASI SO$_2$ data, as shown in Figure 3-.
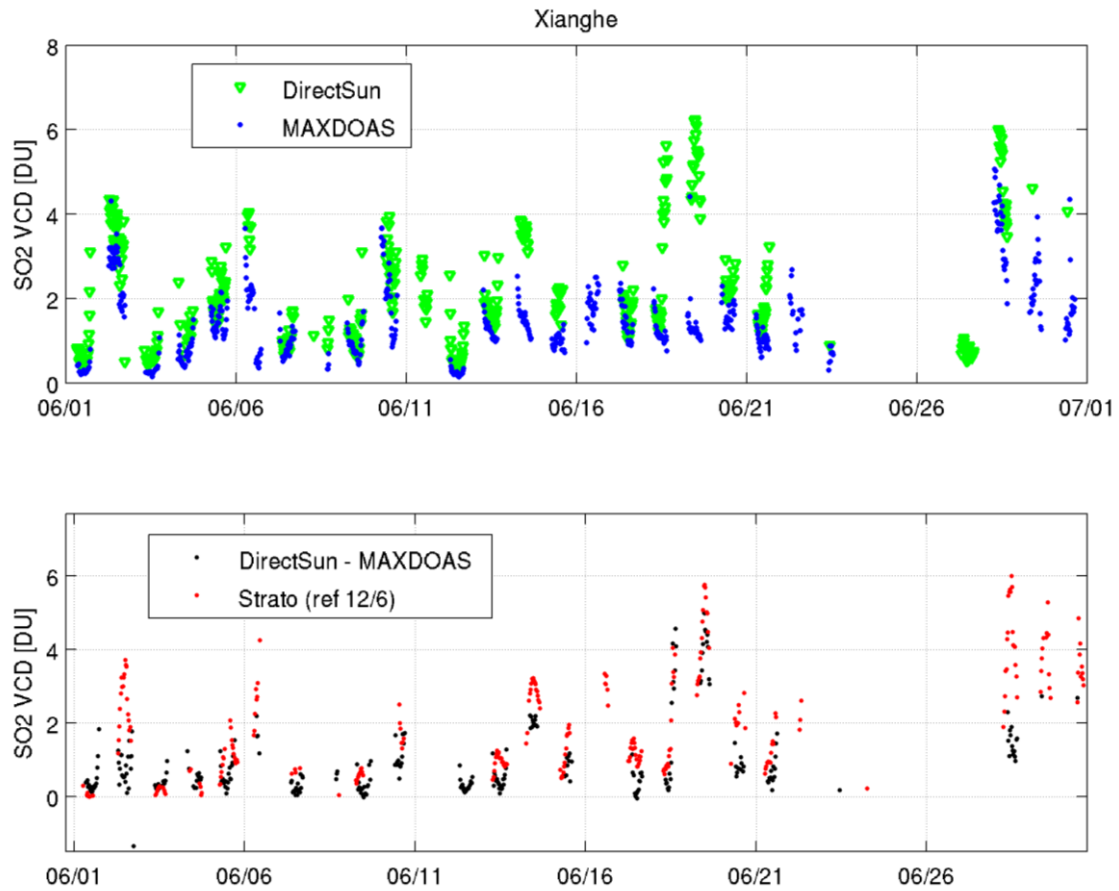
Figure 3-6. SO$_2$ VCD comparisons at Xianghe focusing on June 2011. The first panel shows total SO$_2$ from directSun geometry (in green) and tropospheric SO$_2$ VCD from MAXDOAS (in blue). The second panel shows stratospheric SO$_2$, as retrieved from the total minus tropospheric VCD (in black) and as retrieved using a stratospheric AMF from zenith measurements (in red).
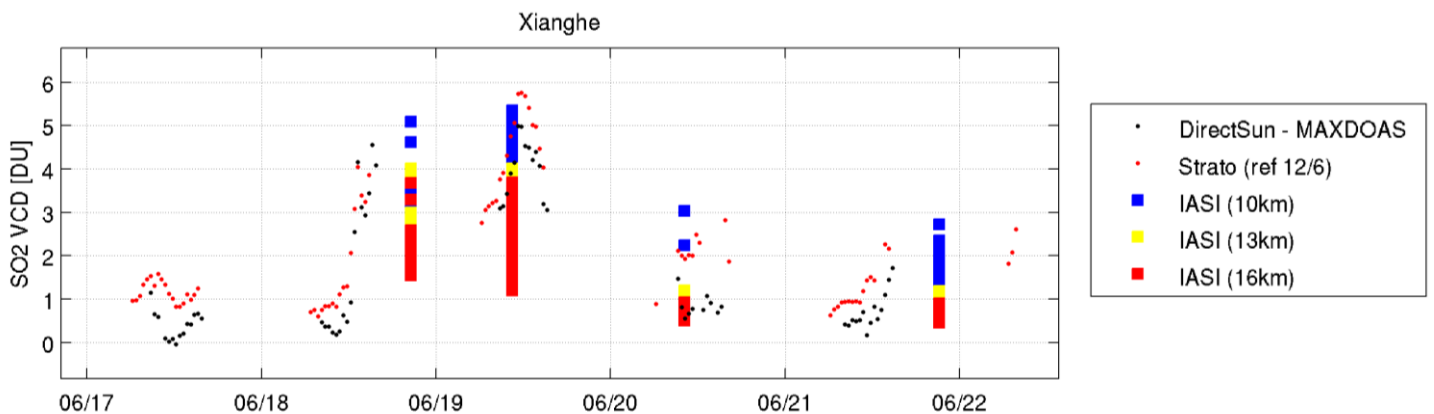
Figure 3-7. SO$_2$ VCD comparisons at Xianghe focusing on June 2011 around the Nabro plume overpass. IASI columns overpasses in a radius of 150km around the stations are reported for 10km, 13km and 16km, and the stratospheric VCD are estimated from the total DirectSun minus tropospheric MAXDOAS VCD (in black) and from zenith measurements with a fixed DOAS reference taken on 12/06/2011 at noon (in red).

In order to compare to IASI VCD day by day more in detail, we need an estimation of the Nabro plume height over the station. The IASI plume height for this eruption has been estimated from IASI in Clarisse et al., 2014 and is of about 16km around the Xianghe station on the 19 June 2011 (Clarisse et al., 2014, figure 10). The IASI columns at 16km within a radius of 80km around the Xianghe station are thus compared day by day in figures 3.8 to 3.11 to the ground-based data. It can be seen that:

- the ground-based signal increases in the afternoon of 18/6/2011, from 2 to 4DU, to be compared with the 1.5-2.5DU seen by IASI in the evening overpass;

- a stable to increasing signal on 19/6/2011 with 3 to 6DU is seen by the ground-based, and 2 to 4DU are seen by IASI during the morning overpass, with larger values for pixels west of the station;

- on the following days the SO_2 signal is reduced: values are between 1 and 2DU on 20 and 21 June from the ground-based, and signal of less than 1DU is seen by IASI on a small number of pixels (~3 every day) at a distance between 30 to 70km of the station.
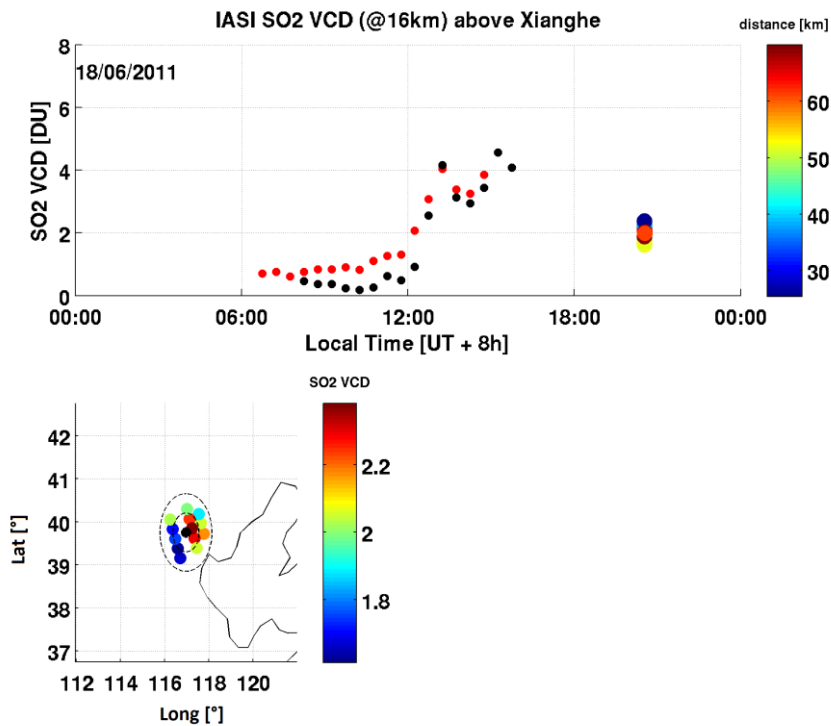
Figure 3-8. SO_2 VCD comparisons at Xianghe focusing on the 18 June 2011. In the first panel, the SO_2 VCD time-series are reported from the total DirectSun minus tropospheric MAXDOAS (in black), from the zenith measurements (in red) and from IASI (columns at 16km, color-coded as a function of the station distance). The second panel presents the geographical distribution of the IASI SO_2 VCD in a radius of 80km around the Xianghe station (circles at 50km and 100km are plotted in dotted lines).
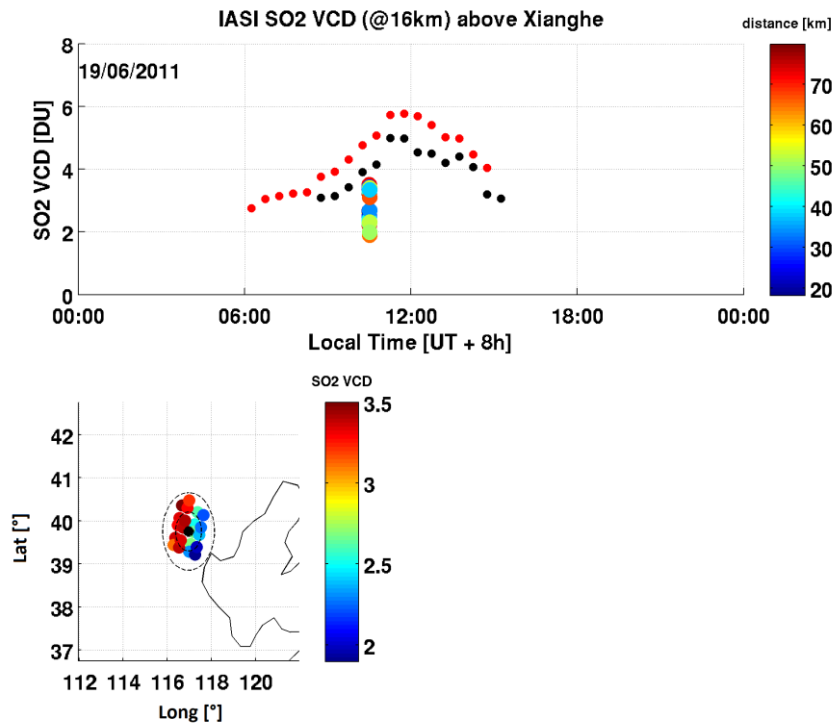
Figure 3-9. As Figure 3-, but for 19 June 2011.
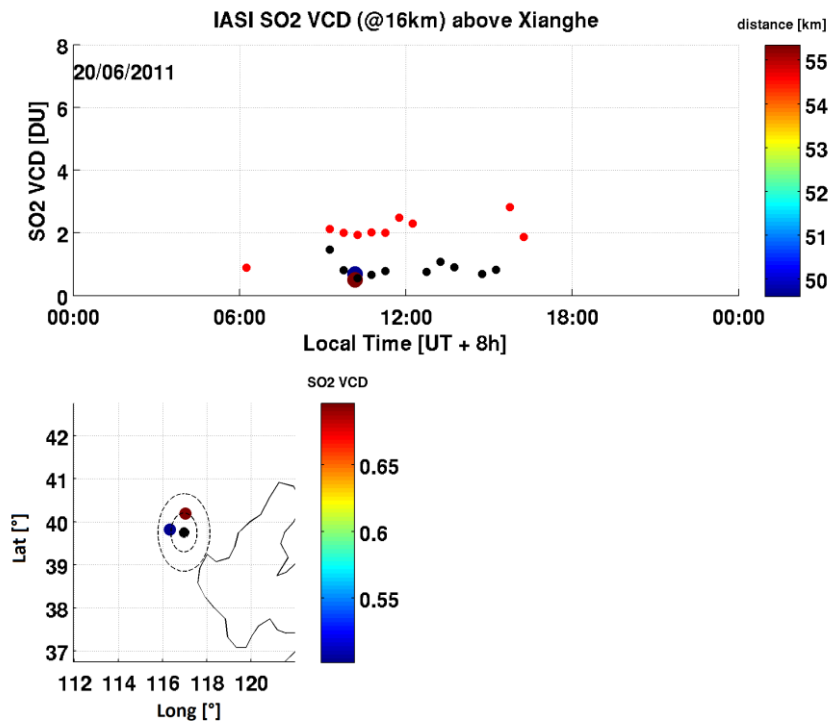
Figure 3-10. As Figure 3-, but for 20 June 2011.
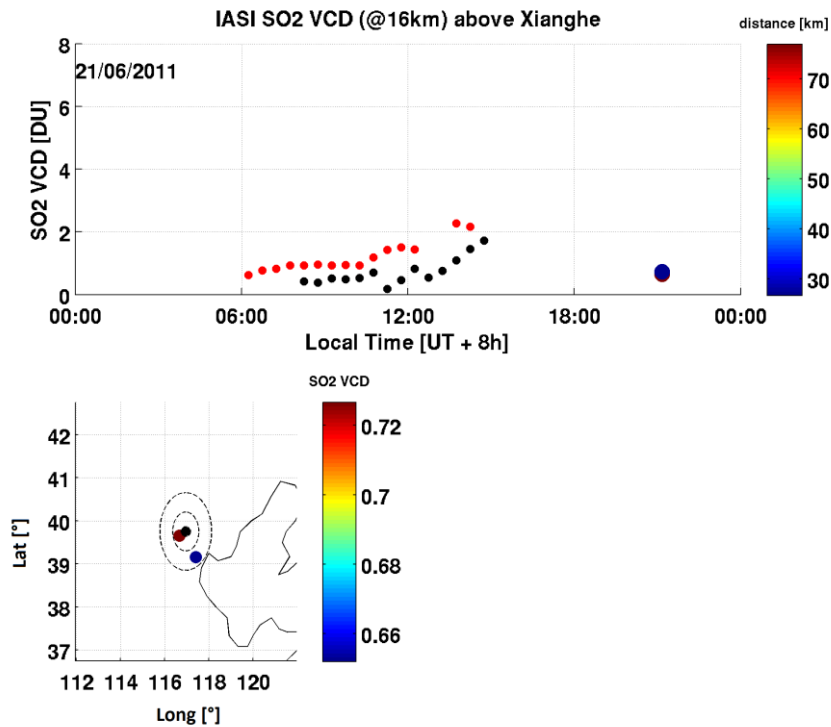
Figure 3-11. As Figure 3-, but for 21 June 2011.

Uccle

The Uccle station is challenging because the instrument measuring in the 2011-2016 period is a commercial mini-MAXDOAS system from Hoffmann (Gielen et al., 2014) and the SO_2 retrieval is quite noisy. An SO_2 signal could be seen by the instrument during the Bardabunga eruption in 2014 (Boichu et al., 2016, figure 9) and we tried to analyse the May-June 2011 period of the Grimsvotn eruption.

Figure 3- presents the stratospheric VCD estimated from the zenith measurements using formula (2) and using a reference spectrum on 6 June. The ground-based time-series shows an enhanced SO_2 signal on 1st of June and 6 and 11 June, which corresponds partially to the SO_2 signals seen by IASI (31 May, 1 June and 10 and 11 June).

In order to compare to IASI VCD day by day more in detail, we need an estimation of the Grimsvotn plume height over the station. The Grimsvotn eruption has been studied in details in Moxnes et al., 2014 and Prata et al., 2017, and showed a separation of the ash and the SO_2 plume during the eruption on 22 May. The height of the SO_2 plume has been estimated at around 10km (Prata et al., 2017, figure 6), while the ash was lower (~4 to 5km). The IASI columns at 10km within a radius of 80km around the Uccle station are thus compared day by day in Figure 3- and Figure 3- to the ground-based data.
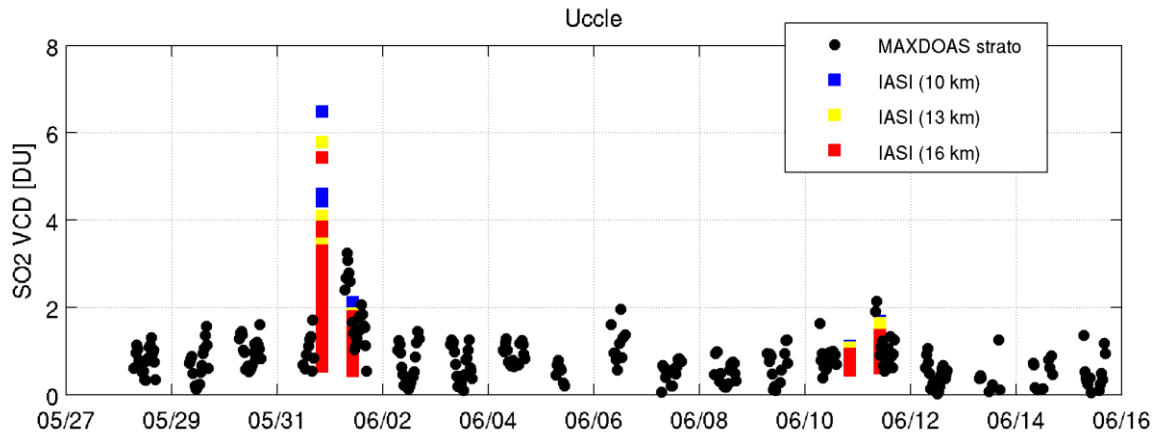
Figure 3-4. Stratospheric SO$_2$ VCD at Uccle focusing on and May-June 2011 during the Grimsvotn eruption.
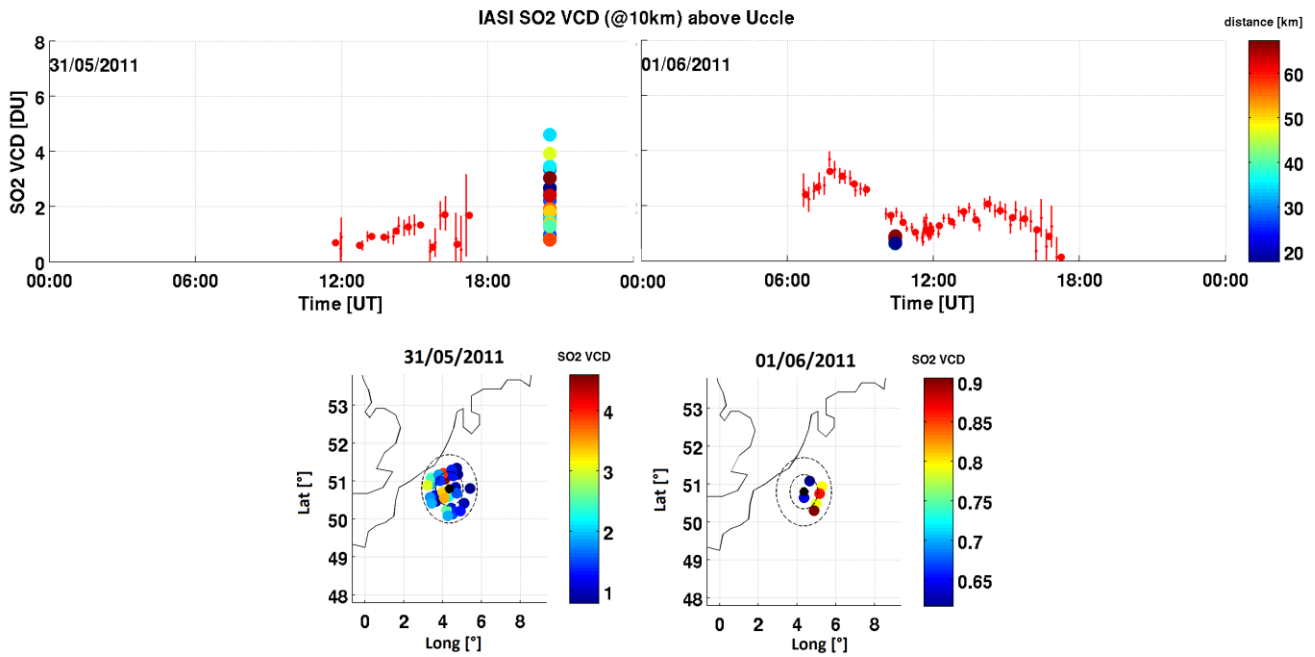
Figure 3-5. SO$_2$ VCD comparisons at Uccle focusing on the 31 May and 01 June 2011. In the upper panels, the SO$_2$ VCD time-series are reported from the zenith measurements (in red) and from IASI (columns at 10km, color-coded as a function of the station distance). The lower panels present the geographical distribution of the IASI SO$_2$ VCD in a radius of 80km around the Uccle station (circles at 50km and 100km are plotted in dotted lines).
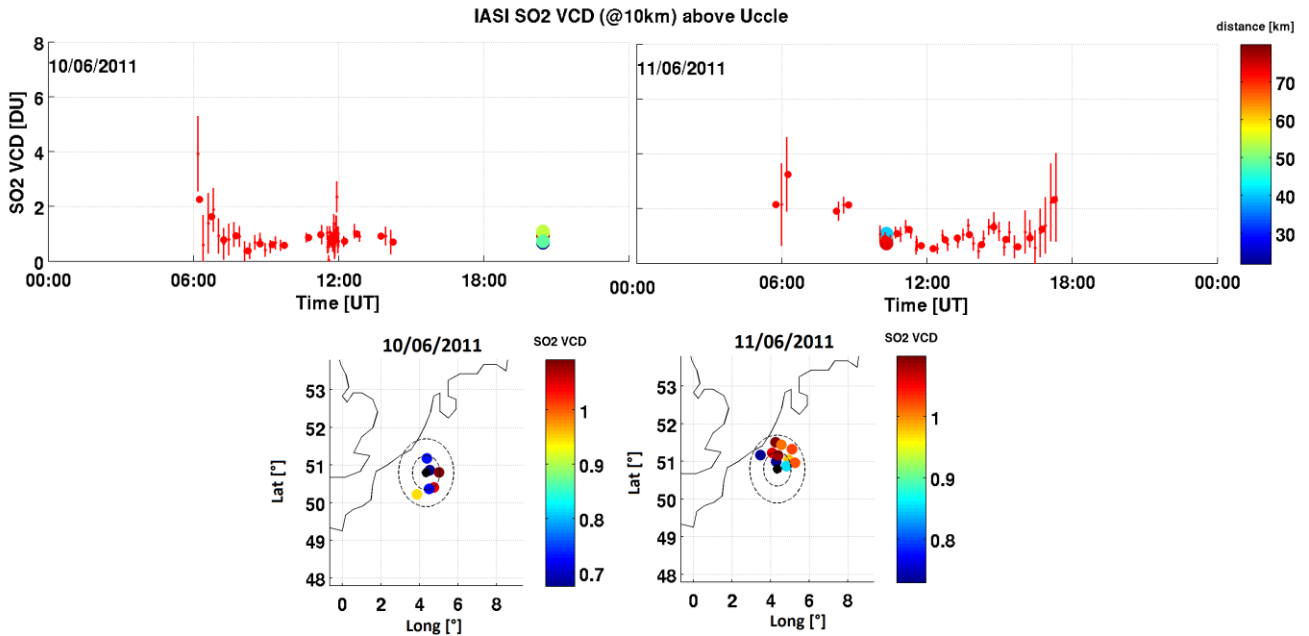
Figure 3-6. As Figure 3-, but for 10 and 11 June 2011.

Figure 3- presents the increase of the SO_2 in the afternoon of 31 May, as seen from the ground-based (from around 1DU to ~2DU), the IASI evening (~21h30) overpass (ranging from ~1DU to 4DU) and the reduction of the SO_2 values in the morning of the 1st June, down to ~1DU, still seen by the morning IASI overpass, but not anymore in the evening overpass. IASI does not see any SO_2 signal again until the evening overpass of 10 June and morning overpass of 11 June (~1DU), as shown in Figure 3-. The ground-based data do not show a very pronounced volcanic signal on those days, except maybe the first points of the 11 June, around 06 UT where the SO_2 VCD are between 2 and 3DU. Their error bars (the DOAS fit error) are however quite large for those points, as often for larger SZA.

4. IASI/METOPA OFL AERIS COMPARISONS AGAINST OMI/AURA OBSERVATIONS

The OMI/Aura SO_2 volcanic load observations at 7km and 15km discussed in this section are the ones provided by Theys et al., 2015a and Theys et al., 2017 and discussed therein. Positive SO_2 columns greater than 0.75 D.U. were extracted on a daily basis and gridded as per the technique discussed in Koukouli et al., 2016. For the 7km SO_2 plume altitude product a restriction was imposed for very high clouds [cloud top pressure < 400 mbars and cloud fraction > 50%] as advised by the data providers which excluded all those pixels from further analysis. A 0.25°x0.25° grid was chosen so as to adapt both OMI and IASI/A instruments onto the same grid and render plotting and numerical comparisons possible. Due to the fact that the OMI pixel size varies depending on the row index position of the measurement, between ~15x25km and ~15x100km, the SO_2 load reported by OMI was weighted by the actual OMI pixel size before the gridding onto the 25x25km grid box was applied. As discussed extensively Theys et al., 2015a, since June 2007, the OMI radiance data is affected by the so-called row anomaly[6] which is due to a partial blockage affecting the nadir-viewing port of the sensor. This anomaly changes with time and position on the orbit and is included as a flag in the OMI operational L1B product. However, the identifying process has a tendency to classify more pixels as affected than strictly necessary; in Theys et al., 2015a, a new identification technique of row anomaly-affected pixels in included. To summarize Section 2.2 of the same paper, the selection is based on fitting residuals over a latitude band around the equator (10°S–10°N), which show typically anomalous high values for the affected rows. A given row is classified as affected by the row anomaly if the mean residual over the equator is larger than the corresponding residual averaged for all rows, by more than 20%. This row anomaly filtering is proven to be a good compromise between the number of retained observations and the data quality.

Out of the approximately 1600 daily data files provided by the ESPRI Data Centre, approximately 800 where daytime IASI/A orbits, within a few hours of the OMI overpass time, and almost half of those had more a few valid pixels for the entire globe. Out of the six different SO_2 columns provided in the IASI/A OFL Aeris files, the SO_2 column which applies to the 7km, 10km, 13km as well as 16km fixed altitude of the algorithm were chosen for further investigation. The days when both IASI and OMI provide enough data points for a meaningful comparison were matched against known volcanic eruptions. The ones enumerated in Table 4 will be discussed further on. A pictorial representation of volcanic eruptions between 2003 and 2014 with known atmospheric SO_2 load impact are shown in Figure 4-1, as per Figure 5 of Carn et al., 2016.

---

[6] http://www.knmi.nl/omi/research/product/rowanomaly-background.php
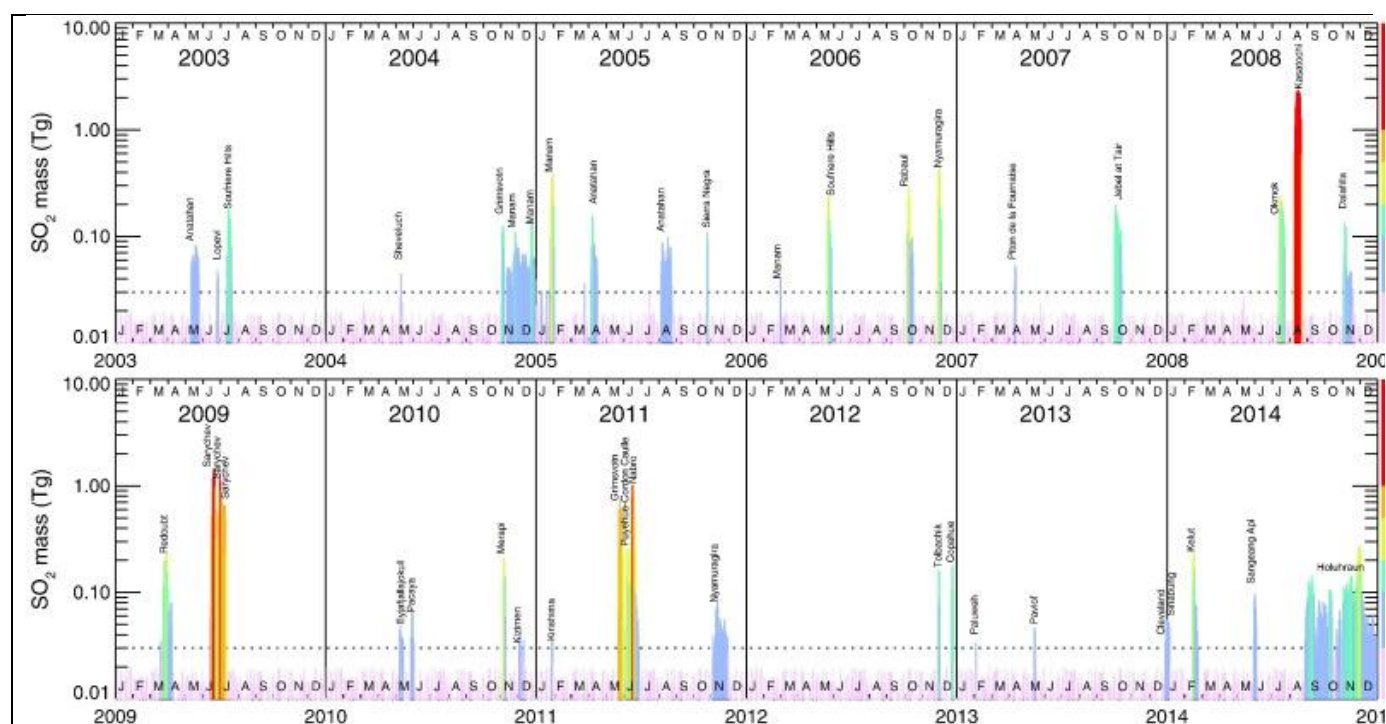
Figure 4-1. Time-series of UTLS SO$_2$ emissions (Tg, log scale) detected by AIRS/Aqua in 2003–2014 using the Prata and Bernardo (2007) SO$_2$ retrieval technique. Sources of the observed SO$_2$ emissions are indicated. As per Figure 5 from Carn et al., 2016.

Table 4. The time periods of common IASI/A OFL Aeris and OMI observations of known volcanic plumes chosen for further study [first two columns] with the volcano name and location in the final two columns.

Date [YYYYMMDD]

Beginning	End	Volcano Name	Country
20071003	20071007	Jebel al Tair	Yemen
20080511	20080514	Mt. Etna	Italy
20080718	20080719	Okmok	Alaska
20080811	20080906	Kasatoschi	Alaska
20081105	20081112	Dalafilla	Ethiopia
20090619	20090716	Sarychev Peak	Russia
20100515	20100520	Eyjafjallajokull	Iceland
20110523	20110604	Grimsvotn	Iceland
20110618	20110627	Nabro	Eritrea
20111105	20111117	Niryacongo	DR Congo
20121223	20121231	Copahue	Chile

Three examples of the gridded datasets created for the purposes of this report, discussed further on, are shown in Figure 4-2 for the OMI/BIRA [upper panels] and IASI/MetopA OFL AERIS [lower panels] SO$_2$ in D.U. for a day during the 2007 Yemen [top], the 2008 Kasatochi [middle] and the 2011 Grimsvotn eruptions [bottom.]

Since the two satellite overpass at different local times of ~3h difference with MetopA in a morning orbit [~09:30 L.T.] and Aura in an afternoon orbit [~13:30], and also have different viewing geometries and fields-of-view, it is customary to compare total SO$_2$ masses in grams per observation time. The SO$_2$ in D.U., which in effect are molecules/cm^2, were turned into 10^6 grams, i.e. kt, by multiplying with the molar mass

[M_{SO2}=64], the area of the 0.25°x0.25° grid point, which naturally varies with varying latitude, and dividing by Avogardos' number as follows:.

$$SO_2\ [kt] = \left. \frac{SO_2\ [D.U.] * 2.68 * 10^{16} * M_{SO_2} * area\ of\ grid\ point}{} \right/ N_A$$

In Figure 4-3 example time series of the total SO_2 masses are shown for the Sarychev Peak eruption of 2009 at the top, the Dalafilla eruption of 2008 in the middle and the Kasatoschi eruption of 2008 at the bottom. In this Figure, the SO_2 mass found for all grid cells of the eruptive region was summed up to provide the total SO_2 mass. In the left column, the 7km OMI plume [in black] is compared to the four IASI/A OFL Aeris plumes [in four different colours] whereas in the right column, the 15km OMI plume is similarly compared. The correlation coefficients are insert, colour-coded to match the IASI/A OFL Aeris plumes. In Table 5 the Pearson's correlation coefficients, R, between the OMI SO_2 plumes at 7km [columns 2 to 5] and at 15km [columns 6 to 9] to the IASI/A OFL Aeris plumes for the different eruptions studied are shown. As can be noted, the comparisons are quite promising for all plume heights assumed by the algorithms, with average coefficients ranging around 0.7-0.9 depending on the comparison pair, with the exception of Mt Etna which was not a high altitude eruptive event. The same information may be accessed pictorially via Figure 4-4 where the correlation coefficients are colour-coded per IASI/A OFL Aeris plume and are shown in histogram mode.
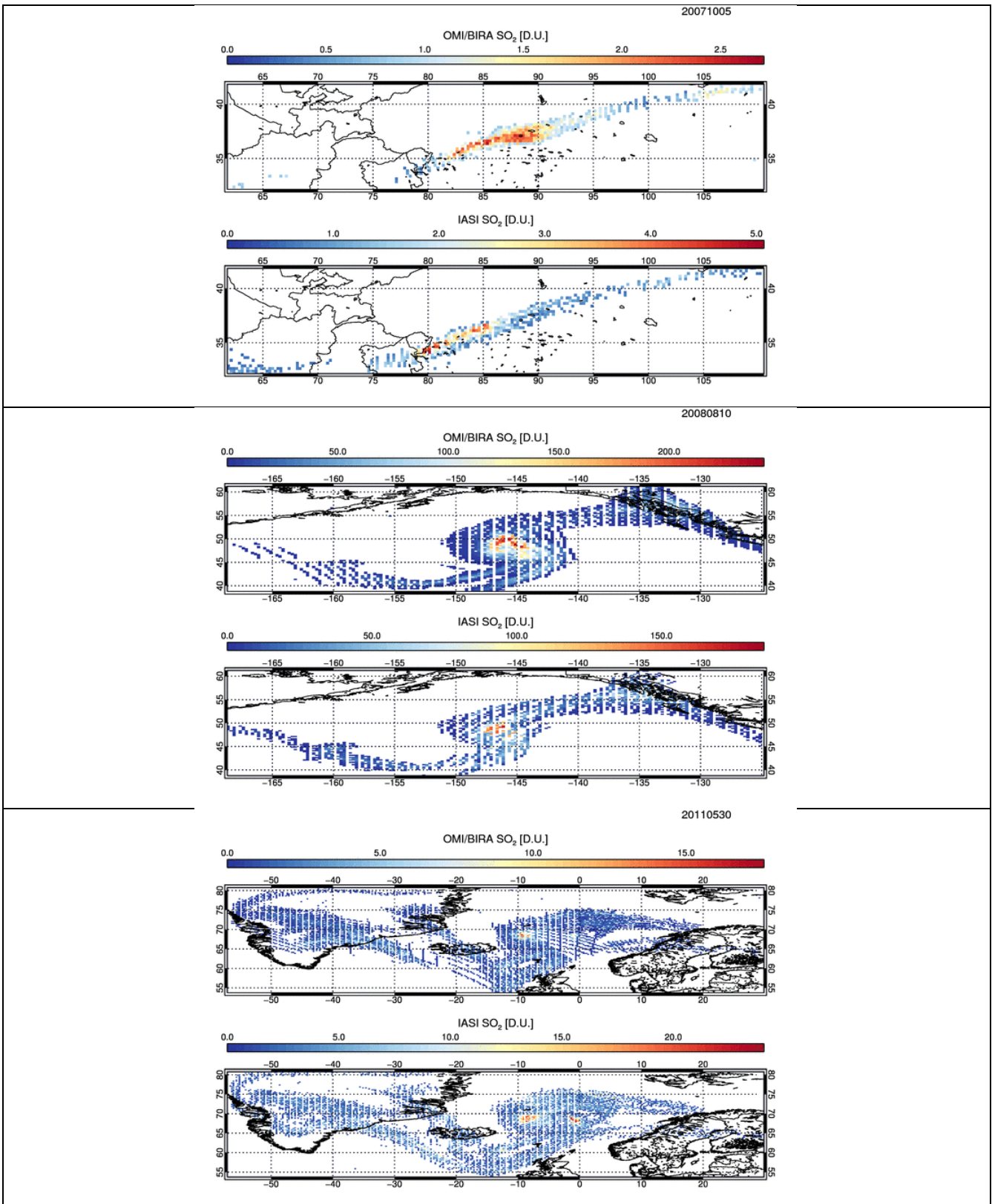
Figure 4-2. Examples of reported total SO₂ columns in D.U. by OMI/BIRA [upper panels] and IASI/MetopA OFL AERIS [lower panels], each at their own observational time, for a single day during the 2007 Yemen [top], the 2008 Kasatochi [middle] and the 2011 Grimsvotn eruptions [bottom.]
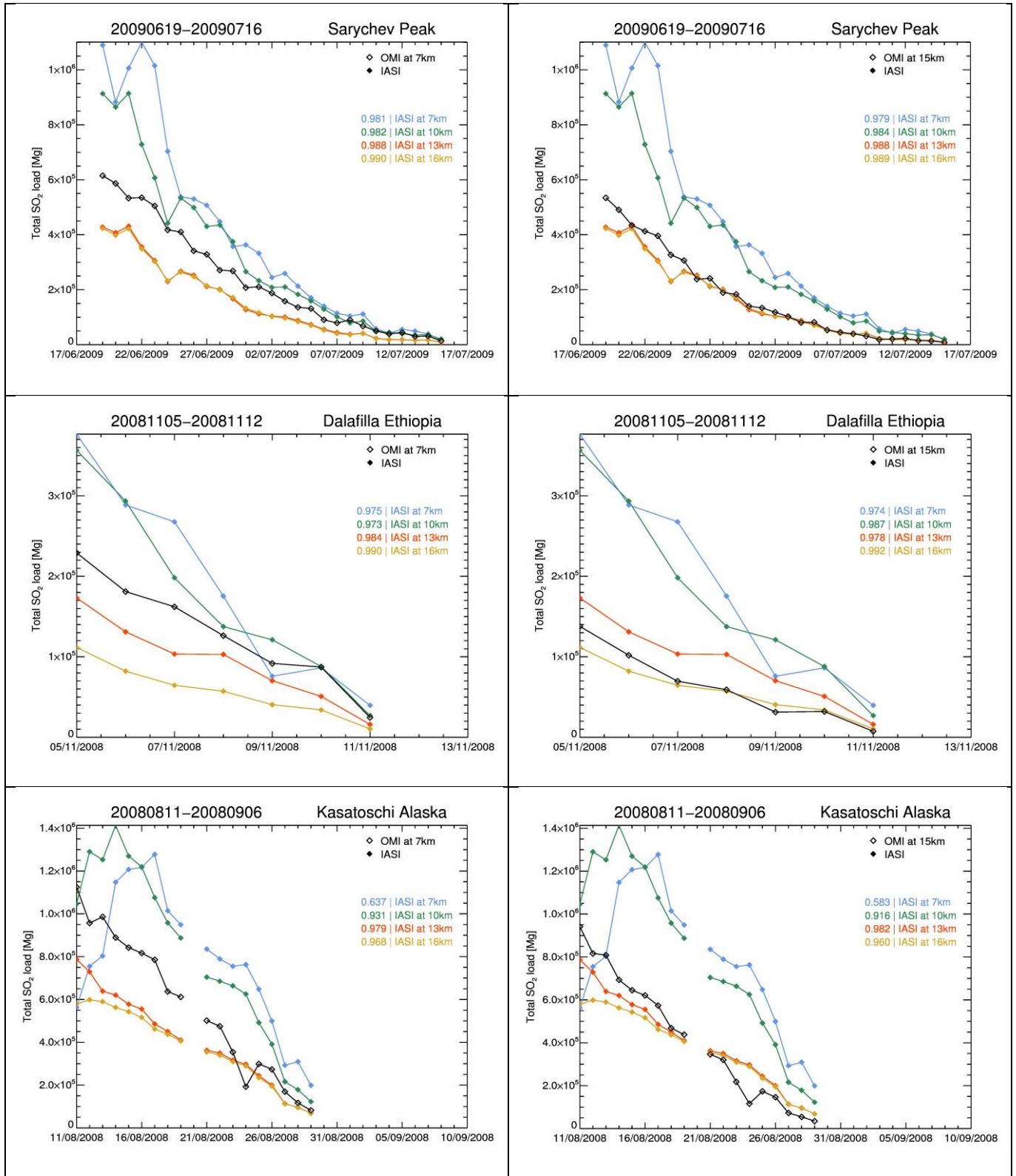
Figure 4-3. Time series of the total SO$_2$ load in 10^6 grams for the 7km OMI plume [left column] and the 15km OMI plume [right column.] In all plots, the OMI plume is shown in black whereas the IASI/A OFL Aeris plumes in four different colours, with the corresponding correlation coefficient also shown. The 2009 Sarychev Peak is shown at the top, the 2008 Dalafilla in the middle and the 2008 Kasatochi eruption at the bottom.

Table 5. Pearson's correlation coefficients between the OMI SO$_2$ plumes at 7km [columns 2 to 5] and at 15km [columns 6 to 9] to the IASI/A OFL Aeris plumes for the different eruptions studied.

Volcanic eruption	OMI at 7km				OMI at 15km			
IASI/A at :	7km	10km	13km	16km	7km	10km	13km	16km
Jebel_al_Tair	0.919	0.83	0.931	0.914	0.978	0.919	0.975	0.976
Mt_Etna	0.034	0.301	0.341	0.421	0.0165	0.292	0.333	0.411
Kasatoschi	0.637	0.931	0.979	0.968	0.583	0.916	0.982	0.96
Dalafilla	0.975	0.973	0.984	0.99	0.974	0.987	0.978	0.992
Sarychev	0.981	0.982	0.988	0.99	0.979	0.984	0.988	0.989
Grimsvotn	0.628	0.78	0.787	0.792	0.742	0.853	0.86	0.861
Nabro	0.786	0.962	0.979	0.975	0.812	0.963	0.98	0.979
Copahue	0.372	0.425	0.404	0.386	0.616	0.644	0.649	0.638
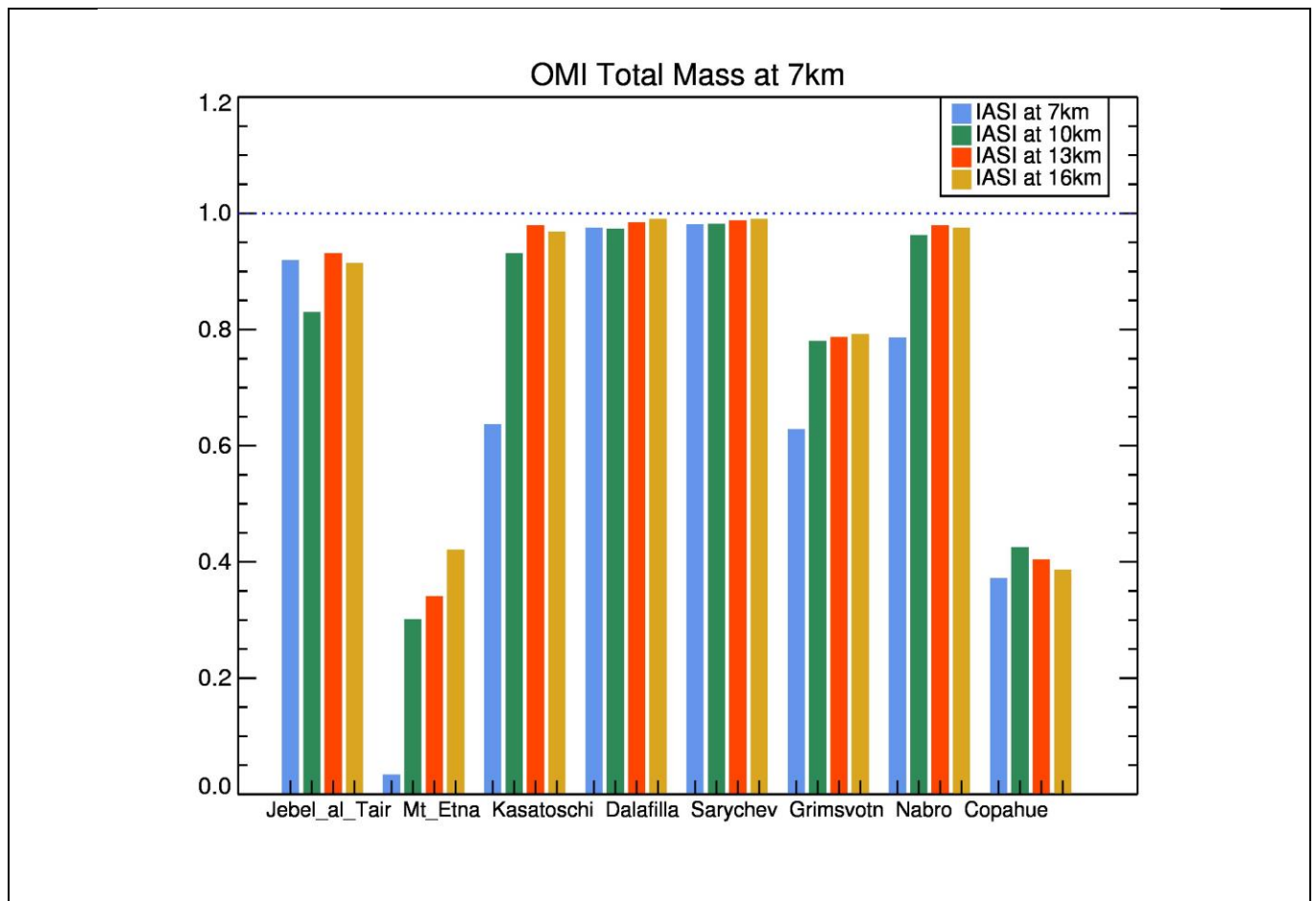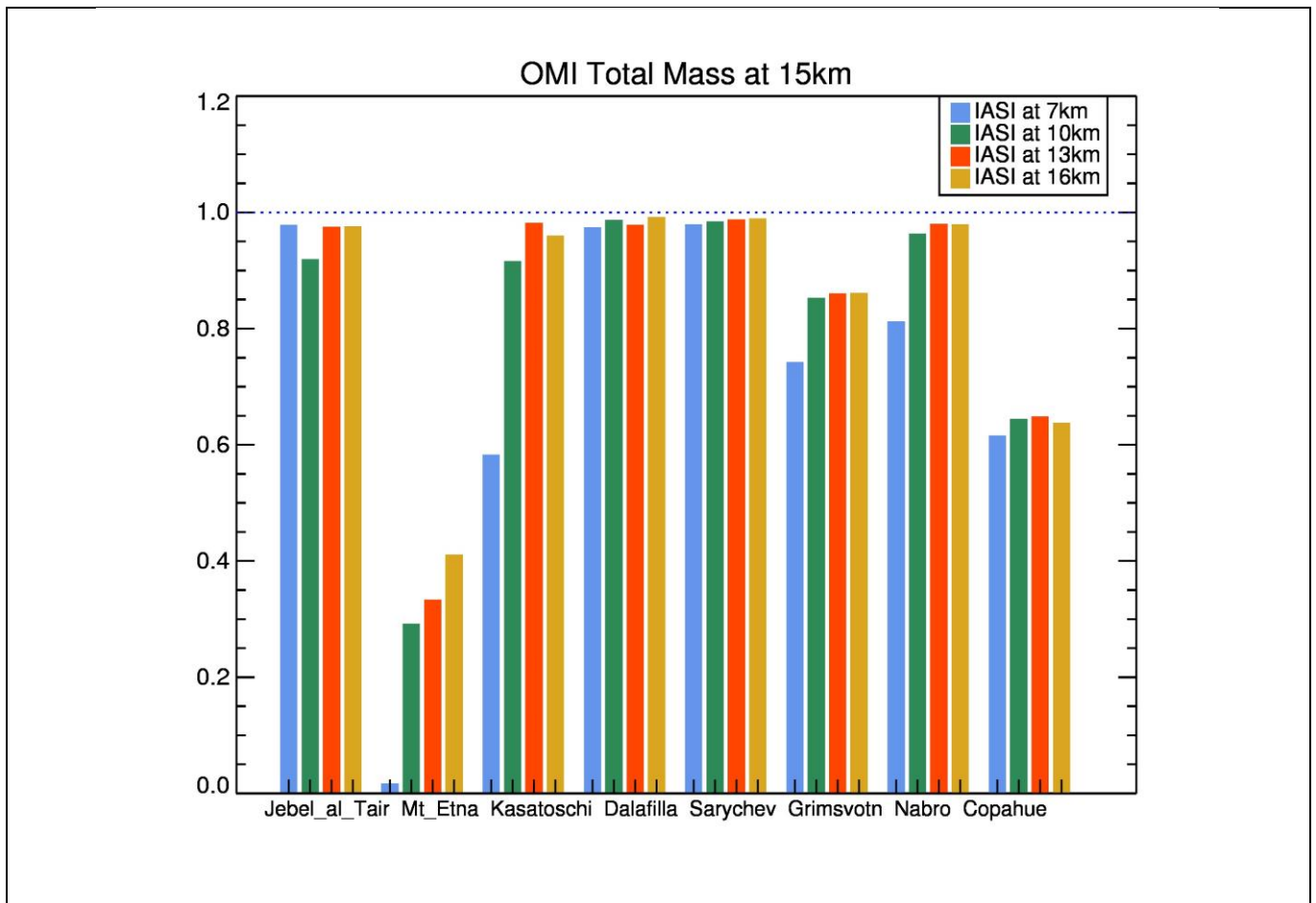
Figure 4-4. Pearson's correlation coefficients between the IASI/A OFL Aeris SO$_2$ masses [in colours] and OMI 7km SO$_2$ mass [upper plot] and 15km SO$_2$ masses [lower plot] for the different eruptions shown in the x-axis title.

We can also examine the ratio between the OMI and the IASI/A OFL Aeris SO$_2$ masses, as a measure of the bias between the absolute atmospheric loadings observed by the two satellite instruments. Ratios with values greater than 2 [ie. 100% bias] where cropped in Figure 4-5. This line of investigation further reveals that the OMI 15km SO$_2$ plume compared favourably to the IASI/A OFL Aeris 13km, as well as the 15km, SO$_2$ plumes.
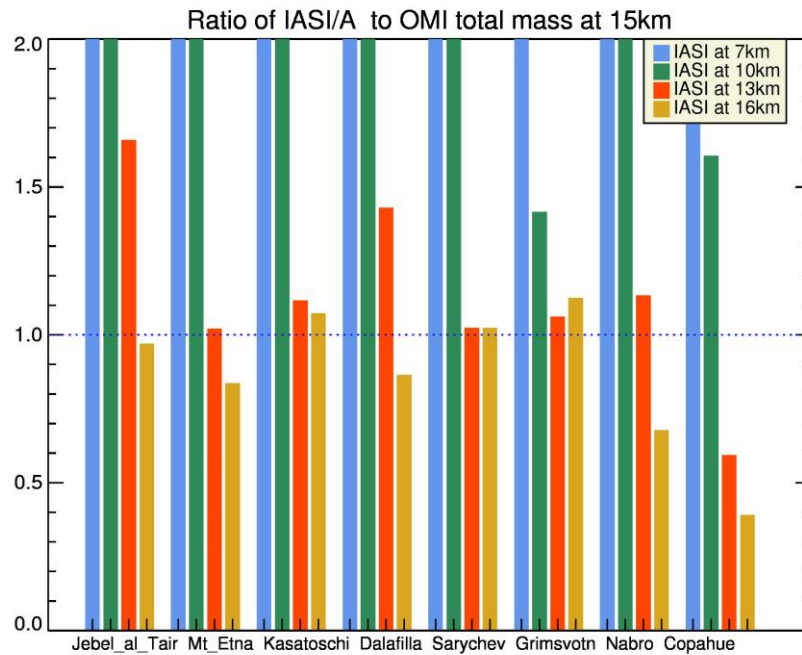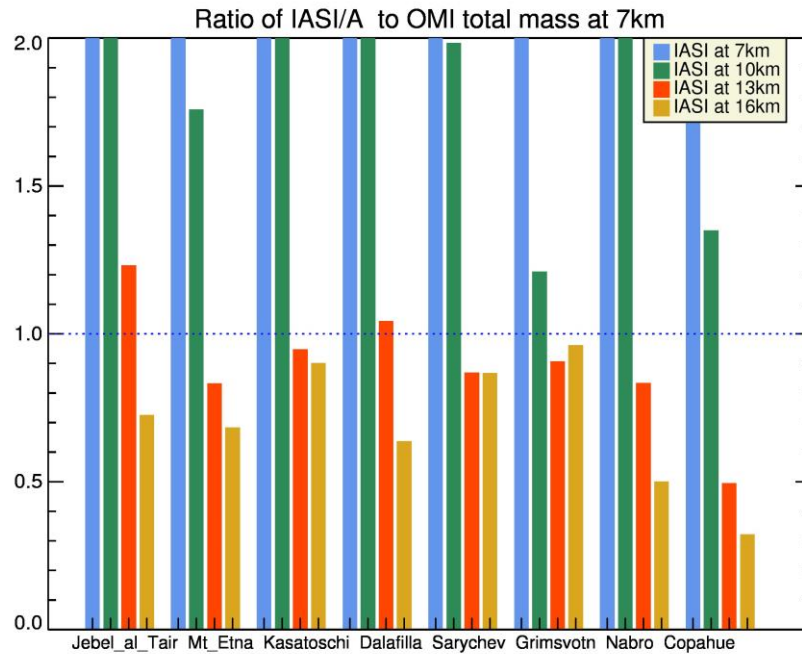
Figure 4-5. Ratio between the IASI/A OFL Aeris SO$_2$ masses and OMI 7km SO$_2$ mass [upper plot] and 15km SO$_2$ masses [lower plot] for the different eruptions shown in the x-axis title.

5. IASI/METOPA OFL AERIS COMPARISONS AGAINST GOME2/METOPA GDP4.8

OBSERVATIONS

In the framework of EUMETSAT's Satellite Application Facility on Atmospheric Composition, AC-SAF, acsaf.org/index.html, GOME-2/MetopA & /MetopB SO_2 total column data products, as well as associated cloud parameters, are delivered in near real time and off-line. Those data products are generated at DLR from MetOp-A and MetOp-B GOME-2 measurements using the UPAS environment version 1.3.9, the level-0-to-1 v5.x and v6.0 processor and the level-1-to-2 GDP v4.8 DOAS retrieval processor [Hassinnen et al., 2016]. For details on the products refer to the GOME2 SO_2 GDP4.8 Validation Report [Theys et al., 2015b]. The GOME2 GDP4.8 total SO_2 column measurements contain four different column products: one assuming the SO2 load is of pure anthropogenic origin, at 1km, one located near the planetary boundary layer at 2.5km altitude, one assuming the SO_2 is located in the free troposphere at 6km altitude and one assuming the SO_2 has volcanic eruptive provenance at 15km altitude. For the following comparisons, the 6km and 15km products are utilized. The GDP4.8 data were filtered as follows: the volcanic flag provided was raised, denoting pixels associated with volcanic SO2 being identified by the GDP4.8 algorithm; only forward scans of the descending orbit were used with associated error smaller than 100%; quality flags of the higher quality and solar zenith angle of < 75°. The columns where then gridded and transformed into masses, as described above for the OMI/Aura observations.

In Figure 5-1, the temporal evolution of three volcanic eruptions during the period of the IASI OFL Aeris dataset is shown for both [daytime] IASI/A and GOME2A, as per Figure 4-3, also normalized per grid cell and area chosen. The agreement is in general good, with high correlation coefficients even though the biases are higher than the corresponding comparisons with the OMI/BIRA datasets. This basically points to the fact that all satellite observations are able to capture the peak and the evolution of the atmospheric SO_2 load after a strong eruption, however due to differences in algorithm parametrizations and, possibly, viewing geometries , they appear to disagree as to the magnitude of the loading. This is a common finding in nearly all works that compare SO_2 loadings from different sensors mainly due to the different algorithms used, see for e.g. Figures 1 & 2 from Koukouli et al., 2014. Even within the same algorithm, the plume height assessed may vary by a large amount [Figure 12 of Carboni et al., 2016]. These variations are currently acceptable by the atmospheric community and do not pose an issue against ORR requirements. In Table 6 the correlations for all eligible eruptions discussed is shown and with the notable exception of the three-day Mt Etna outgassing event, these are found to be quite satisfactory.
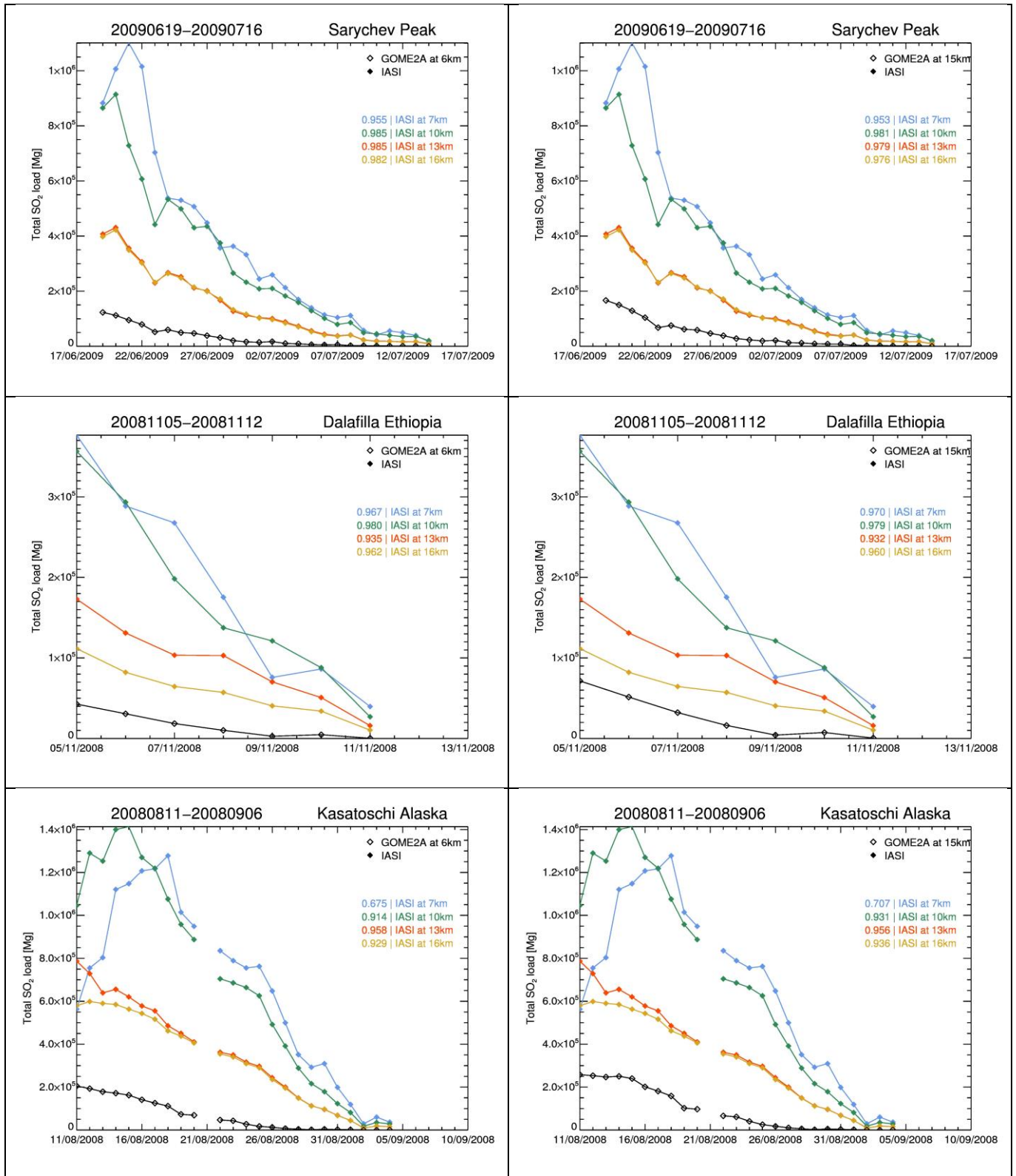
Figure 5-1. Time series of the total SO_2 load in 10^6 grams for the 6km GOME2A plume [left column] and the 15km GOME2A plume [right column.] In all plots, the OMI plume is shown in black whereas the IASI/A OFL Aeris plumes in four different colours, with the corresponding correlation coefficient also shown. The 2009 Sarychev Peak is shown at the top, the 2008 Dalafilla in the middle and the 2008 Kasatochi eruption at the bottom.

Table 6. Pearson's correlation coefficients between the GOME2A SO$_2$ plumes at 6km [columns 2 to 5] and at 15km [columns 6 to 9] to the IASI/A OFL Aeris plumes for the different eruptions studied.

Volcanic eruption	GOME2A at 6km				GOME2A at 15km			
IASI/A at :	7km	10km	13km	16km	7km	10km	13km	16km
Jebel_al_Tair	0.989	0.962	0.969	0.98	0.977	0.95	0.948	0.964
Kasatoschi	0.675	0.914	0.958	0.929	0.707	0.931	0.956	0.936
Dalafilla	0.967	0.98	0.935	0.962	0.97	0.979	0.932	0.96
Sarychev	0.955	0.985	0.985	0.982	0.953	0.981	0.979	0.976
Eyjafjallajokull	0.836	0.903	0.836	0.892	0.846	0.905	0.849	0.892
Grimsvotn	0.876	0.904	0.897	0.903	0.881	0.872	0.869	0.871
Nabro	0.806	0.954	0.969	0.968	0.822	0.959	0.972	0.972
Niryacongo	0.793	0.843	0.946	0.959	0.863	0.904	0.938	0.947

6. IASI/MᴇᴛᴏᴘA & /MᴇᴛᴏᴘB NRT_PPF_ᴠ6.3 ᴄᴏᴍᴘᴀʀɪsᴏɴs ᴀɢᴀɪɴsᴛ OMI/Aᴜʀᴀ OBSERVATIONS

As already described in Section 1.2 as well as Section 3, the BRESCIA algorithm has been applied in EUMETSAT and IASI/MetopA and /MetopB data have become available via EUMETCAST since June 20th 2017. In Figure 6-1 the locations of the valid SO$_2$ columns corresponding to 16km plumes for a BT difference of greater than 1K are shown in purple and greater than 2K are shown in red, for MetopA in the upper and MetopB in the lower panels. The time span of this composite image is June 20th to October 30th 2017 inclusive. As can be noted, the stricter criterion entirely obfuscates the erroneous SO$_2$ detections over the highly reflective Antarctic regions. It is known that no major eruption occurred during this time period, apart from a small eruption in the Galapagos islands, on the 5th of September and the Tinakula eruption in the Solomon Islands between the 21st and 23rd of October.
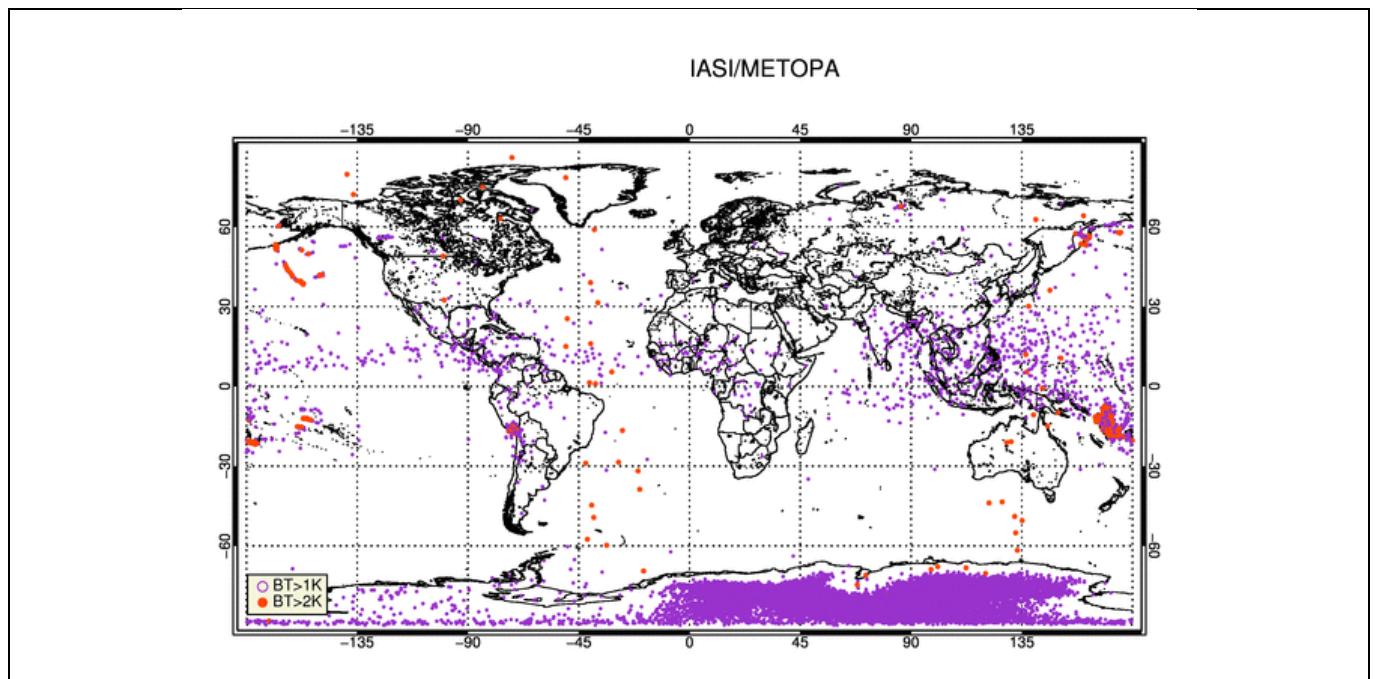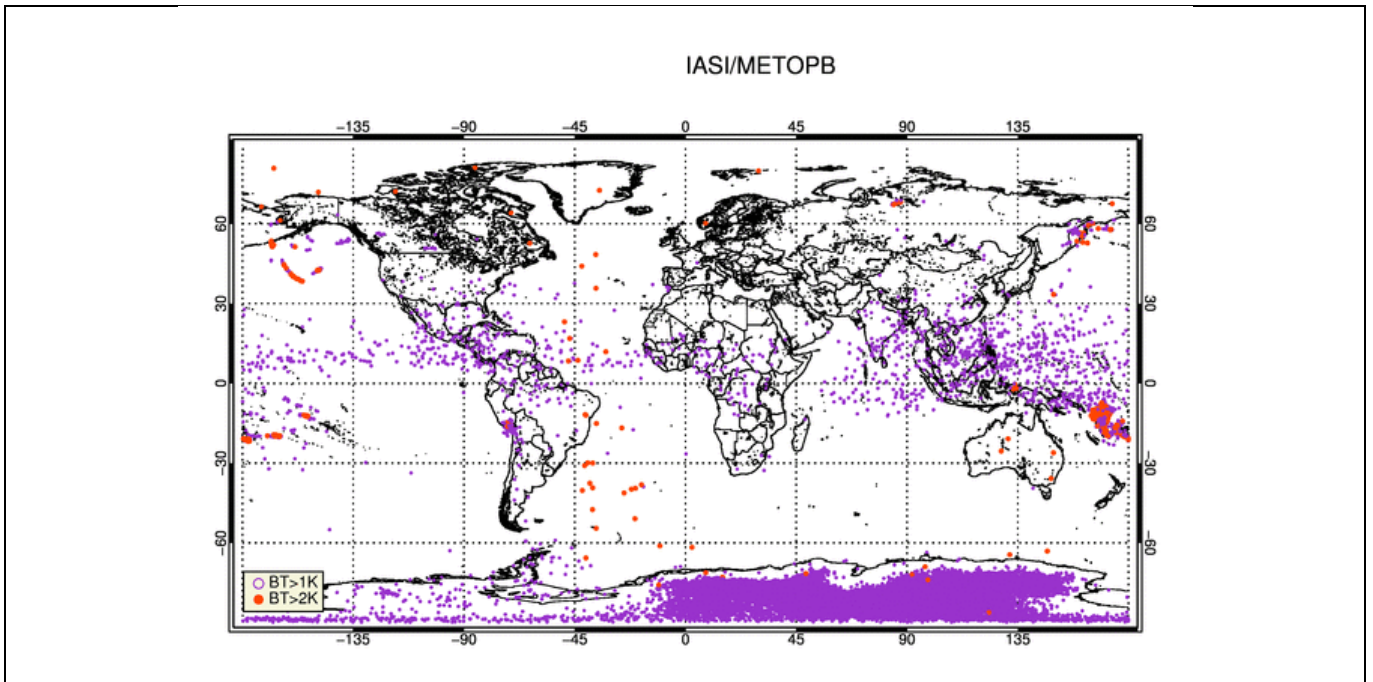
Figure 6-1. The EUMETSAT NRT_PPF_v6.3 IASI plumes at 16km for MetopA [top] and MetopB [bottom.] All IASI SO$_2$ data with associated brightness temperature differences above 1K are shown in the purple open circles, whereas above 2K are shown in red filled dots.
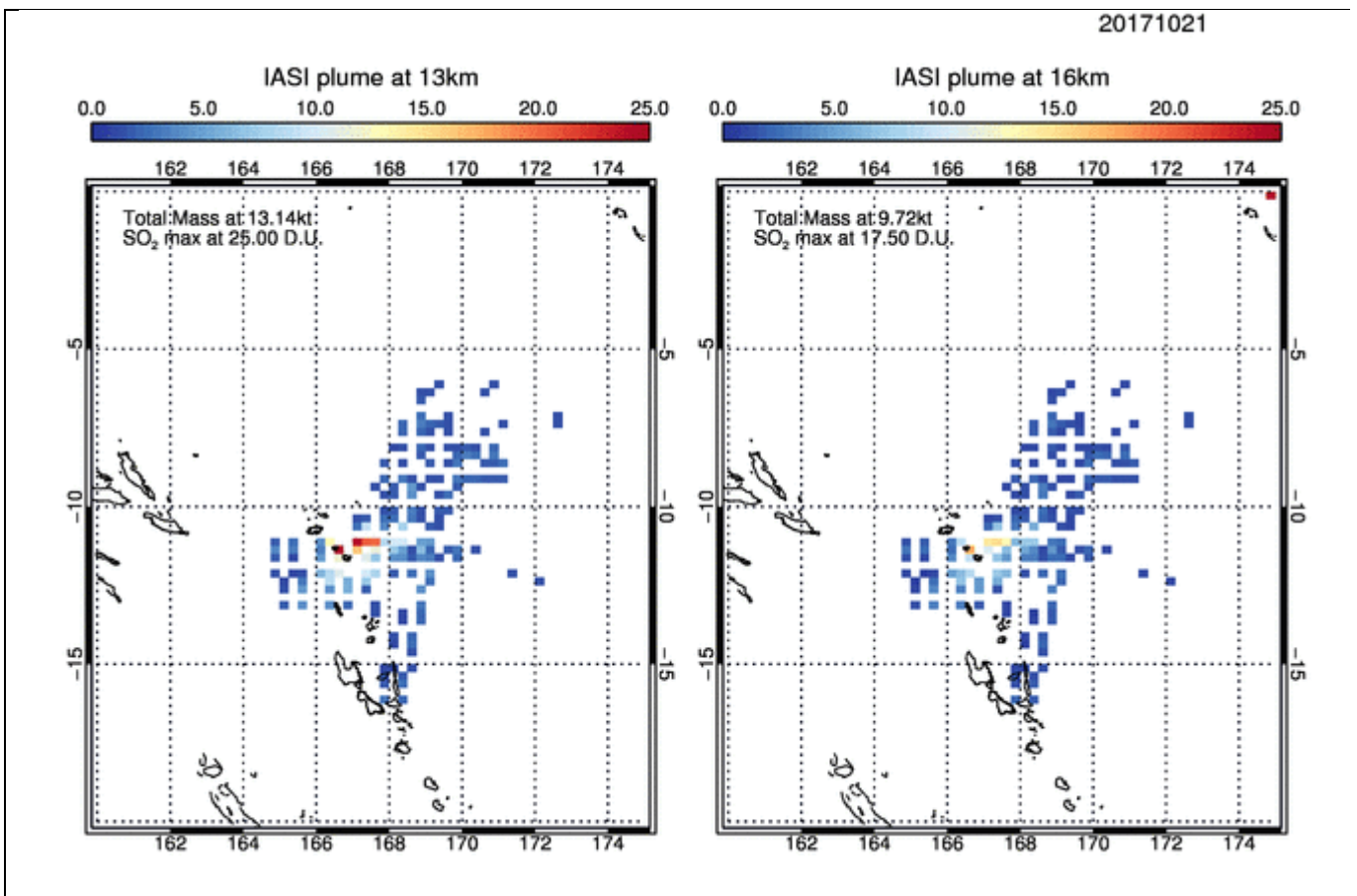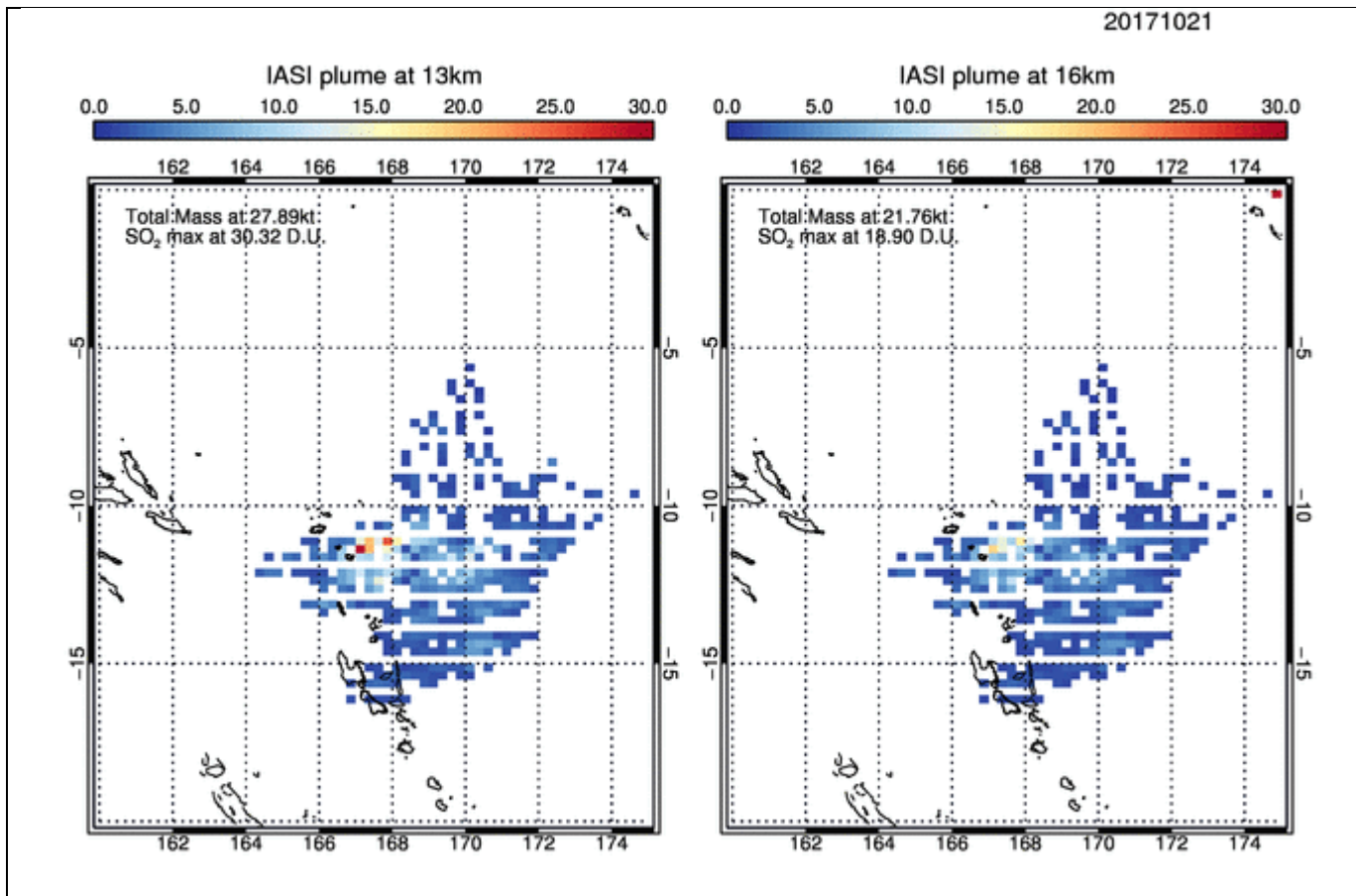
Figure 6-2. The EUMETSAT NRT_PPF_v6.3 IASI plumes at 13km [left column] and 16km [right column] for MetopA [top] and MetopB [bottom] for the Tinakula, Solomon Islands, eruption. The total mass calculated as well as the max SO₂ load in DU are also shown insert.

In Figure 6-2 the EUMETSAT NRT_PPF_v6.3 IASI plumes at 13km [left column] and 16km [right column] for MetopA [top] and MetopB [bottom] for the Tinakula, Solomon Islands, eruption. The total mass calculated as well as the max SO₂ load in DU are also shown insert. For comparison and to show the overall agreement, the image provided by NASA's Global Sulfur Dioxide Monitoring Home Page[7], is reproduced in Figure 6-3. Differences in absolute masses can easily be attributed to differences in the post-treatment of the two datasets.

---

[7] https://so2.gsfc.nasa.gov/omi_2004_now.html
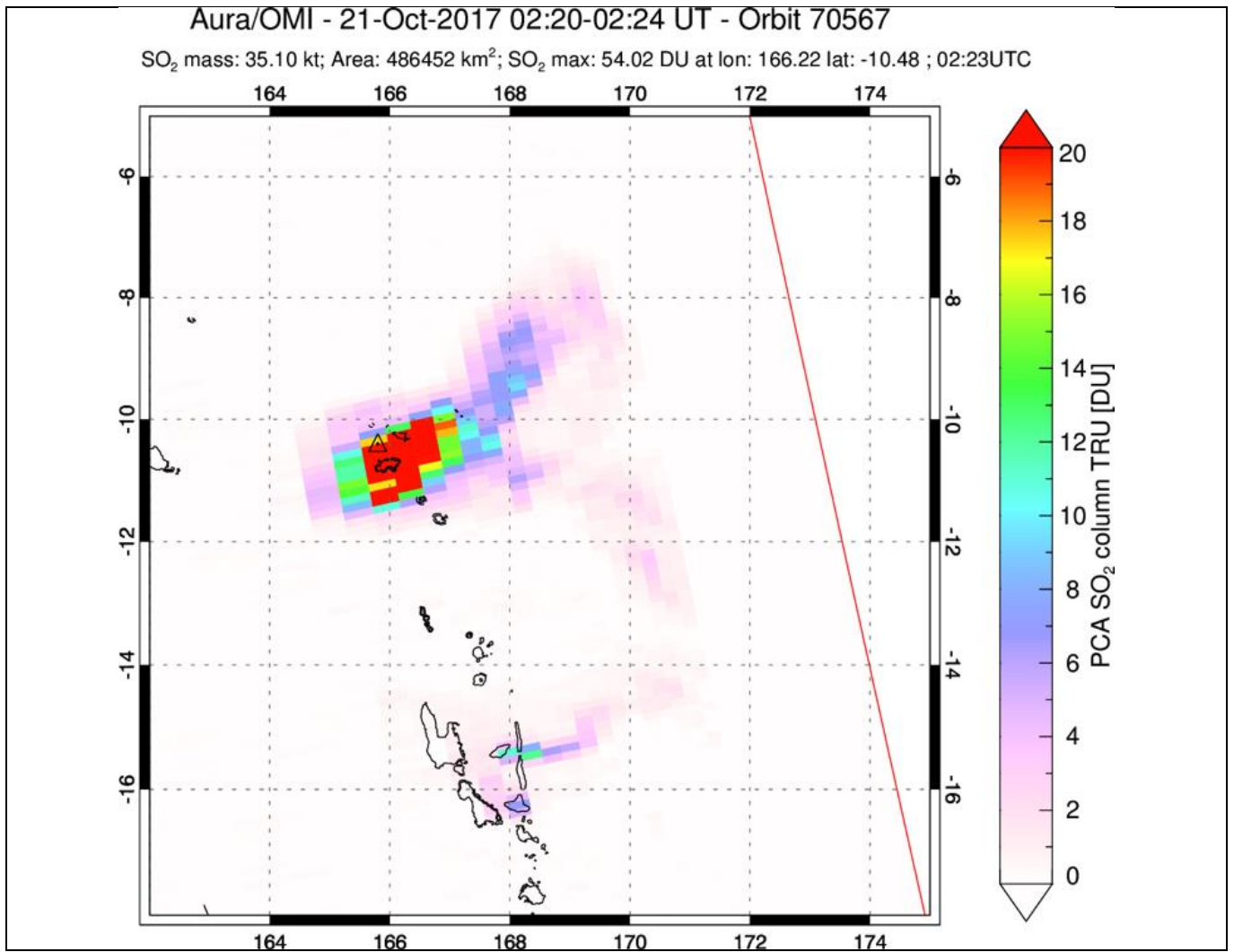
Figure 6-3. The TRU OMI/Aura NASA SO_2 product for the Tinakula, Solomon Islands, eruption on the 21st of October 2017. The total mass calculated as well as the max SO_2 load in DU are also shown insert. Image from NASA's volcanic SO_2 gallery, https://so2.gsfc.nasa.gov/pix/special/2017/tina/tinakula_20171021_omi.html.

7. CONCLUSIONS

In the framework of EUMETSAT's Satellite Application Facility on Atmospheric Composition Monitoring (AC SAF, formerly O3M SAF), SO_2 total column data products have been generated using the Brescia v201510 algorithm operating at both LATMOS and EUMETSAT facilities as observed by the IASI instrument on board the MetOp-A and B platforms.

This report investigates the quality of the IASI/MetopA (2007-2013) and IASI/MetopA & /MetopB (June – October 2017) SO_2 columns by comparing them to ground-based measurements performed on a global scale by Brewer and MAXDOAS spectrophotometers, as well as satellite observations obtained by the OMI/Aura and GOME2/MetopA instruments. Different spatiotemporal collocation criteria were applied depending on the comparisons as well as different restriction criteria. The report is focused solely on SO_2 of volcanic provenance, and mainly from eruptive events at that.

Out of fifty Brewer spectrophotometers that report SO_2 loading globally, 35 had collocations within 50km from an IASI overpass. Due to the locations of the most active volcanoes in remote areas, few Brewer instruments were able to capture SO_2 plumes created by the major volcanic events of the 2007-2013. It is shown that while the signal of the ground-based measurement rises above the noise levels inherent in the Brewer algorithm, those levels never reach the satellite reported ones [also seen in comparison with other satellite instruments.]

Out of seven MAXDOAS spectrophotometers deployed globally, three provide meaningful collocations to the IASI overpasses, the ground-based stations generally show enhanced SO_2 signals just before/during/after the enhanced IASI SO_2 overpasses and the order of magnitude of the SO_2 signals is well comparable.

Eleven major eruptive events were analysed in detail vis-a-vis the loadings observed by IASI/MetopA & /MetopB in comparison to OMI/Aura and GOME2/MetopA. Different assumptions in plume heights within the equivalent algorithms were all considered. The analysis on SO_2 masses showed that, for the entire eruption episodes, the correlations range between 0.70 and 0.95 depending on the plume height and satellite instrument. The IASI 13 & 16km plumes show the best agreement to the OMI/Aura 15km plume mostly within ±20%.

We hence conclude that the target accuracy of 100% is achieved below 10km whereas the optimal accuracy of 50% is achieved above 10km for the EUMETSAT NRT_PPF_v6.3 IASI plumes.

REFERENCES

Athanassiadou, M., Francis, P. N., Saunders, R. W., Atkinson, N. C., Hort, M. C., Havemann, S., Thelen, J.-C. and Bush, M. (2016), A case study of sulphur dioxide identification in three different volcanic eruptions, using Infrared satellite observations (IASI). Met. Apps, 23: 477–490. doi:10.1002/met.1572

Bauduin, S., Clarisse, L., C. Clerbaux, D. Hurtmans, and P.-F. Coheur, IASI observations of sulfur dioxide (SO_2) in the boundary layer of Norilsk, J. Geophys. Res. Atmos., 119, 4253–4263, doi:10.1002/2013JD021405, 2014.

Bauduin, S., Clarisse, L., Hadji-Lazaro, J., Theys, N., Clerbaux, C., and Coheur, P.-F.: Retrieval of near-surface sulfur dioxide (SO_2) concentrations at a global scale using IASI satellite observations, Atmos. Meas. Tech., 9, 721-740, doi:10.5194/amt-9-721-2016, 2016.

Boichu, M., Chiapello, I., Brogniez, C., Péré, J.-C., Thieuleux, F., Torres, B., Blarel, L., Mortier, A., Podvin, T., Goloub, P., Sohne, N., Clarisse, L., Bauduin, S., Hendrick, F., Theys, N., Van Roozendael, M., and Tanré, D.: Current challenges in modeling far-range air pollution induced by the 2014-15 BÃ¡rdarbunga fissure eruption (Iceland), Atmos. Chem. Phys., 16, 10831-10845, doi:10.5194/acp-16-10831-2016, 2016.

Boynard, A., et al., First simultaneous space measurements of atmospheric pollutants in the boundary layer from IASI: A case study in the North China Plain, Geophys. Res. Lett., 41, 645–651, doi:10.1002/2013GL058333, 2014.

Brenot, H., Theys, N., Clarisse, L., van Geffen, J., van Gent, J., Van Roozendael, M., van der A, R., Hurtmans, D., Coheur, P.-F., Clerbaux, C., Valks, P., Hedelt, P., Prata, F., Rasson, O., Sievers, K., and Zehner, C.: Support to Aviation Control Service (SACS): an online service for near-real-time satellite monitoring of volcanic plumes, Nat. Hazards Earth Syst. Sci., 14, 1099-1123, https://doi.org/10.5194/nhess-14-1099-2014, 2014.

Carboni, E., Grainger, R. G., Mather, T. A., Pyle, D. M., Thomas, G. E., Siddans, R., Smith, A. J. A., Dudhia, A., Koukouli, M. E., and Balis, D.: The vertical distribution of volcanic SO_2 plumes measured by IASI, Atmos. Chem. Phys., 16, 4343-4367, doi:10.5194/acp-16-4343-2016, 2016.

Carn, S. A., Clarisse, L. and Prata, A. J.: Multi-decadal satellite measurements of global volcanic degassing, J. Volcanol. Geotherm. Res., 311, 99–134, doi:10.1016/j.jvolgeores.2016.01.002, 2016.

Clarisse, L., Coheur, P. F., Prata, A. J., Hurtmans, D., Razavi, A., Phulpin, T., Hadji-Lazaro, J., and Clerbaux, C.: Tracking and quantifying volcanic SO_2 with IASI, the September 2007 eruption at Jebel at Tair, Atmos. Chem. Phys., 8, 7723-7734, doi:10.5194/acp-8-7723-2008, 2008.

Clarisse, L., Hurtmans, D., Clerbaux, C., Hadji-Lazaro, J., Ngadi, Y., and Coheur, P.-F.: Retrieval of sulphur dioxide from the infrared atmospheric sounding interferometer (IASI), Atmos. Meas. Tech., 5, 581-594, doi:10.5194/amt-5-581-2012, 2012.

Clarisse, L., Coheur, P.-F., Theys, N., Hurtmans, D., and Clerbaux, C.: The 2011 Nabro eruption, a SO_2 plume height analysis using IASI measurements, Atmos. Chem. Phys., 14, 3095-3111, doi:10.5194/acp-14-3095-2014, 2014.

Clemer, K., Van Roozendael, M., Fayt, C., Hendrick, F., Hermans, C., Pinardi, G., Spurr, R., Wang, P., and De Maziere, M.: Multiple wavelength retrieval of tropospheric aerosol optical properties from MAXDOAS measurements in Beijing, Atmos. Meas. Tech., 3, 863-878, 2010.

Clerbaux, C., Boynard, A., Clarisse, L., George, M., Hadji-Lazaro, J., Herbin, H., Hurtmans, D., Pommier, M., Razavi, A., Turquety, S., Wespes, C., and Coheur, P.-F.: Monitoring of atmospheric composition using the thermal infrared IASI/MetOp sounder, Atmos. Chem. Phys., 9, 6041-6054, doi:10.5194/acp-9-6041-2009, 2009.

Fioletov, V. E., McLinden, C. A., Krotkov, N., Li, C., Joiner, J., Theys, N., Carn, S., and Moran, M. D.: A global catalogue of large SO2 sources and emissions derived from the Ozone Monitoring Instrument, Atmos. Chem. Phys., 16, 11497-11519, doi:10.5194/acp-16-11497-2016, 2016.

Gielen, C., Van Roozendael, M., Hendrick, F., Pinardi, G., Vlemmix, T., De Bock, V., De Backer, H., Fayt, C., Hermans, C., Gillotay, D., and Wang, P.: A simple and versatile cloud-screening method for MAX-DOAS retrievals, Atmos. Meas. Tech., 7, 3509-3527, doi:10.5194/amt-7-3509-2014, 2014.

Gielen, C., Hendrick, F., Pinardi, G., De Smedt, I., Fayt, C., Hermans, C., Stavrakou, T., Bauwens, M., Muller, J.-F., Ndenzako, E., Nzohabonayo, P., Akimana, R., Niyonzima, S., Van Roozendael, M., and De Maziere, M.: Characterisation of Central-African aerosol and trace-gas emissions based on MAX-DOAS measurements and model simulations over Bujumbura, Burundi, Atmos. Chem. Phys. Discuss., doi:10.5194/acp-2016-1104, in review, 2017.

Hassinen, S., Balis, D., Bauer, H., Begoin, M., Delcloo, A., Eleftheratos, K., Gimeno Garcia, S., Granville, J., Grossi, M., Hao, N., Hedelt, P., Hendrick, F., Hess, M., Heue, K.-P., Hovila, J., Jønch-Sørensen, H., Kalakoski, N., Kauppi, A., Kiemle, S., Kins, L., Koukouli, M. E., Kujanpää, J., Lambert, J.-C., Lang, R., Lerot, C., Loyola, D., Pedergnana, M., Pinardi, G., Romahn, F., van Roozendael, M., Lutz, R., De Smedt, I., Stammes, P., Steinbrecht, W., Tamminen, J., Theys, N., Tilstra, L. G., Tuinder, O. N. E., Valks, P., Zerefos, C., Zimmer, W., and Zyrichidou, I.: Overview of the O3M SAF GOME-2 operational atmospheric composition and UV radiation data products and data availability, Atmos. Meas. Tech., 9, 383-407, https://doi.org/10.5194/amt-9-383-2016, 2016.

Hendrick, F., Van Roozendael, M., Chipperfield, M. P., Dorf, M., Goutail, F., Yang, X., Fayt, C., Hermans, C., Pfeilsticker, K., Pommereau, J.-P., Pyle, J. A., Theys, N., and De Maziere, M.: Retrieval of stratospheric and tropospheric BrO profiles and columns using ground-based zenith-sky DOAS observations at Harestua, 60° N, Atmos. Chem. Phys., 7, 4869-4885, doi:10.5194/acp-7-4869-2007, 2007.

Hendrick, F., Mahieu, E., Bodeker, G. E., Boersma, K. F., Chipperfield, M. P., De Mazière, M., De Smedt, I., Demoulin, P., Fayt, C., Hermans, C., Kreher, K., Lejeune, B., Pinardi, G., Servais, C., Stübi, R., van der A, R., Vernier, J.-P. and Van Roozendael, M.: Analysis of stratospheric NO_2 trends above Jungfraujoch using ground-based UV-visible, FTIR, and satellite nadir observations, Atmos. Chem. Phys., 12(18), 8851–8864, doi:10.5194/acp-12-8851-2012, 2012.

Hendrick, F., Muller, J.-F., Clamer, K., Wang, P., De Maziere, M., Fayt, C., Gielen, C., Hermans, C., Ma, J. Z., Pinardi, G., Stavrakou, T., Vlemmix, T., and Van Roozendael, M.: Four years of ground-based MAX-DOAS observations of HONO and NO2 in the Beijing area, Atmos. Chem. Phys., 14, 765-781, doi:10.5194/acp-14-765-2014, 2014.

Honninger, G., von Friedeburg, C. and Platt, U.: Multi axis differential optical absorption spectroscopy (MAX-DOAS), Atmos. Chem. Phys., 4, 231–254 [online] Available from: www.atmos-chem-phys.org/acp/4/231/, 2004.

Höpfner, M., Boone, C. D., Funke, B., Glatthor, N., Grabowski, U., Günther, A., Kellmann, S., Kiefer, M., Linden, A., Lossow, S., Pumphrey, H. C., Read, W. G., Roiger, A., Stiller, G., Schlager, H., von Clarmann, T. and Wissmüller, K.: Sulfur dioxide (SO2) from MIPAS in the upper troposphere and lower stratosphere 2002–2012, Atmos. Chem. Phys., 15, 7017–7037, doi:10.5194/acp-15-7017-2015, 2015.

Karagulian, F., L. Clarisse, C. Clerbaux, A. J. Prata, D. Hurtmans, and P. F. Coheur, Detection of volcanic SO2, ash, and H2SO4 using the Infrared Atmospheric Sounding Interferometer (IASI), J. Geophys. Res., 115, D00L02, doi:10.1029/2009JD012786, 2010.

Kerr, J. B., Asbridge, I. A., and Evans, W. F. J.: Intercomparison of Total Ozone Measured by the Brewer and Dobson Spectrophotometers at Toronto, Journal of Geophysical Research, 93, 11129-11140, 1988.

Kerr, J. B.: New methodology for deriving total ozone and other atmospheric variables from Brewer spectrophotometer direct sun spectra, J. Geophys. Res., 107(D23), 4731, doi:10.1029/2001JD001227, 2002.

Kerr, J. B.: The Brewer Spectrophotometer, In UV Radiation in Global Climate Change: Measurements, Modeling and Effects on Ecosystems, W. Gao, D. L. Schmoldt and J. R. Slusser (Eds), Tsinghua University Press, Beijing and Springer-Verlag Berlin Heidelberg, ISBN 978-7-302-20360-5, pp. 160-191, 2010.

Koukouli, M. E., Clarisse, L., Carboni, E., Van Gent J., Spinetti, C., Balis, D., Dimopoulos S., Grainger, R., Theys, N., Tampellini, L., and Zehner, C.: Intercomparison of Metop-A SO_2 measurements during the 2010-2011 Icelandic eruptions, Annals of Geophysics, Fast Track 2, doi: 10.4401/ag-6613, 2014.

Koukouli, M.E., D. S. Balis, R. van der A, et al., Anthropogenic sulphur dioxide load over China as observed from different satellite sensors, Atmospheric Environment, doi:/10.1016/j.atmosenv.2016.09.007, 2016.

Moxnes, E. D., N. I. Kristiansen, A. Stohl, L. Clarisse, A. Durant, K. Weber, and A. Vogel, Separation of ash and sulfur dioxide during the 2011 Grímsvötn eruption, J. Geophys. Res. Atmos., 119, doi:10.1002/2013JD021129, 2014.

Prata, A. J., and C. Bernardo, Retrieval of volcanic SO2 column abundance from Atmospheric Infrared Sounder data, J. Geophys. Res., 112, D20204, doi:10.1029/2006JD007955, 2007 .

Prata, F., Woodhouse, M., Huppert, H. E., Prata, A., Thordarson, T., and Carn, S.: Atmospheric processes affecting the separation of volcanic ash and SO2 in volcanic eruptions: inferences from the May 2011 Grimsvotn eruption, Atmos. Chem. Phys., 17, 10709-10732, https://doi.org/10.5194/acp-17-10709-2017, 2017.

Schmidt, A., S. et al., Satellite detection, long-range transport, and air quality impacts of volcanic sulfur dioxide from the 2014–2015 flood lava eruption at Bárðarbunga (Iceland), J. Geophys. Res. Atmos., 120, 9739–9757, doi:10.1002/2015JD023638, 2015.

Stamoulis, Th., Comparisons of OMI/Aura SO_2 observations with Brewer spectrophotometer ground-based measurements: the 2004-2014 volcanic activity, M.Sci. in Environmental Physics thesis, Laboratory of Atmospheric Physics, Aristotle University of Thessaloniki, Greece, 2016.

Theys, N., Campion, R., Clarisse, L., Brenot, H., van Gent, J., Dils, B., Corradini, S., Merucci, L., Coheur, P.-F., Van Roozendael, M., Hurtmans, D., Clerbaux, C., Tait, S., and Ferrucci, F.: Volcanic SO_2 fluxes derived from satellite data: a survey using OMI, GOME-2, IASI and MODIS, Atmos. Chem. Phys., 13, 5945-5968, doi:10.5194/acp-13-5945-2013, 2013.

Theys, N., I. De Smedt, J. van Gent, T. Danckaert, T. Wang, F. Hendrick, T. Stavrakou, S. Bauduin, L. Clarisse, C. Li, N. Krotkov, H. Yu, H. Brenot, and M. Van Roozendael, Sulfur dioxide vertical column DOAS retrievals from the Ozone Monitoring Instrument: Global observations and comparison to ground-based and satellite data. J. Geophys. Res. Atmos., 120, 2470–2491. doi: 10.1002/2014JD022657, 2015a.

Theys, N., M. Koukouli, G. Pinardi, M. Van Roozendael, D. Balis, P. Hedelt, and P. Valks, O3M-SAF GOME-2 GDP4.8 Sulphur Dioxide Columns Validation Report, SAF/O3M/IASB/VR/SO2/112/TN-IASB-GOME-2-O3MSAF-SO2-2015, available from: http://acsaf.org/docs/vr/Validation_Report_NTO_OTO_DR_SO2_GDP48_Dec_2015.pdf, last accessed: 02 November 2017, 2015b.

van der A, R. J., Mijling, B., Ding, J., Koukouli, M. E., Liu, F., Li, Q., Mao, H., and Theys, N.: Cleaning up the air: effectiveness of air quality policy for SO_2 and NO_x emissions in China, Atmos. Chem. Phys., 17, 1775-1789, doi:10.5194/acp-17-1775-2017, 2017.

Wang, T., Hendrick, F., Wang, P., Tang, G., Clémer, K., Yu, H., Fayt, C., Hermans, C., Gielen, C., Müller, J.-F., Pinardi, G., Theys, N., Brenot, H. and Van Roozendael, M.: Evaluation of tropospheric SO2 retrieved from MAX-DOAS measurements in Xianghe, China, Atmos. Chem. Phys., 14(20), 11149–11164, doi:10.5194/acp-14-11149-2014, 2014.

Zerefos, C. S., et al., Detecting volcanic sulfur dioxide plumes in the Northern Hemisphere using the Brewer spectrophotometers, other networks, and satellite observations, Atmos. Chem. Phys., 17, 551-574, doi:10.5194/acp-17-551-2017, 2017.

Appendix I.

Table 7. The top twenty emitting volcanoes globally in the decade 2005 to 2014 sorted by their reported emission levels [final column]. List extracted from NASA's Global Sulfur Dioxide Monitoring Home Page[8] and Fioletov et al., 2016.

Latitude	Longitude	Name	Country	kt SO$_2$ [total over decade]
-16.25	168.12	Ambrym	Vanuatu	26516
19.42	-155.29	Kilauea	USA	18131
-6.09	155.23	Bagana	Papua New Guinea	13922
-1.41	29.20	Nyamuragira	Democratic Republic of Congo	11999
-15.40	167.83	Aoba	Vanuatu	10463
37.73	15.00	Mt. Etna	Italy	7505
-4.24	152.21	Tavurvur	Papua New Guinea	6943
1.68	127.88	Dukono	Indonesia	6289
19.02	-98.62	Popocatepetl	Mexico	5614
-4.08	145.04	Manam	Papua New Guinea	5439
16.35	145.67	Anatahan	Northern Mariana Islands	5362
16.72	-62.18	Soufriere Hills	Montserrat (UK)	5081
-19.53	169.44	Yasur	Vanuatu	4934
31.59	130.66	Sakura-jima	Japan	4078
34.08	139.53	Miyake-jima	Japan	4047
54.05	159.45	Karymsky	Russia	3243
4.90	-75.32	Nevado del Ruiz	Colombia	3166
11.98	-86.16	Masaya	Nicaragua	3158
29.64	129.72	Suwanose-jima	Japan	3095
52.45	158.20	Mutnovsky	Russia	2949

---

[8] https://so2.gsfc.nasa.gov/

Appendix II.

Table 8. List of Brewer stations that report SO₂ values in the WOUDC repository for the period 2007 to 2013.

WMO station ID	Station name	Latitude	Longitude	Sector
2	Tamanrasset	22.78	5.52	Europe
10	NewDelhi	28.65	77.217	Asia
18	Alert	82.5	-62.32	North America
21	Edmonton	53.55	-114.1	North America
24	Resolute	74.72	-94.98	North America
35	Arosa	46.78	9.68	Europe
53	Uccle	50.8	4.35	Europe
65	Toronto	43.78	-79.47	North America
76	Goose Bay	53.31	-60.36	North America
77	Churchill	58.74	-94.07	North America
95	Taipei	25.04	121.51	Asia
99	Hohenpeissenberg	47.81	11.01	Europe
100	Budapest	47.43	19.18	Europe
111	Amundsen-Scott	-89.99	70.241	Antarctica
123	Yakutsk	62.08	129.75	Middle East & Russia
187	Poona	18.533	73.85	Asia
252	Seoul	37.57	126.98	Asia
261	Thessaloniki	40.52	22.97	Europe
262	Sodankyla	67.37	26.63	Europe
267	Sondrestrom	67	-50.62	Europe
282	Kislovodsk	43.73	42.66	Middle East & Russia
290	Saturna Island	48.77	-123.13	North America
295	Mt Waliguan	36.29	100.9	Asia
301	Ispra	45.8	8.63	Europe
305	Rome University	41.9	12.5	Europe
306	Chengkung	23.099	121.365	Asia
307	Obninsk	55.0986	36.608	Middle East & Russia
308	Madrid	40.45	-3.72	Europe

314	Belgrano II	-77.87	-34.63	Antarctica
315	Eureka	79.99	-85.93	North America
316	De Bilt	52.1	5.18	Europe
318	Valentia	51.93	-10.25	Europe
322	Petaling Jaya	3.1	101.65	Asia
325	Linan	30.3	119.73	Asia
326	Longfengshan	44.73	127.58	Asia
330	Hanoi	21.063	105.82	Asia
331	Poprad Gavonce	49.03	20.32	Europe
332	Pohang	36.03	129.38	Asia
336	Isfahan	32.51	51.71	Middle East & Russia
346	Murcia	38	-1.16	Europe
348	Ankara	39.97	32.863	Middle East & Russia
349	Lhasa	29.67	91.13	Asia
351	King George Island	-62.15	-58.87	South America
352	Manchester	53.47	-2.23	Europe
353	Reading	51.44	-0.94	Europe
376	Mersa Matruh	31.33	27.22	Europe
401	Santa Cruz	28.46	-16.25	Europe
405	La Coruna	43.33	-8.41	Europe
411	Zaragoza	41.634	-0.881	Europe
435	Paramaribo	5.806	-55.215	South America
447	Goddard	38.99	-76.83	North America
468	Cape D'Aguilar	22.21	114.26	Asia
473	Punta Arenas	-53.14	-70.85	South America
475	Bandung	-6.9	107.58	Asia
478	Zhongshan	-69.37	76.38	Asia
479	Aosta	45.74	7.36	Europe
481	Tomsk	56.4833	85.067	Middle East & Russia
499	Princess Elisabeth	-71.95	23.35	Antarctica
512	University Of Toronto	43.66	-79.4	North America
513	Anmyeon-do	36.538	126.33	Asia